
Mémoire

Auteur : Garny, Alexandre

Promoteur(s) : Loicq, Jerome

Faculté : Faculté des Sciences

Diplôme : Master en sciences spatiales, à finalité spécialisée

Année académique : 2020-2021

URI/URL : <http://hdl.handle.net/2268.2/12699>

Avertissement à l'attention des usagers :

Tous les documents placés en accès ouvert sur le site le site MatheO sont protégés par le droit d'auteur. Conformément aux principes énoncés par la "Budapest Open Access Initiative"(BOAI, 2002), l'utilisateur du site peut lire, télécharger, copier, transmettre, imprimer, chercher ou faire un lien vers le texte intégral de ces documents, les disséquer pour les indexer, s'en servir de données pour un logiciel, ou s'en servir à toute autre fin légale (ou prévue par la réglementation relative au droit d'auteur). Toute utilisation du document à des fins commerciales est strictement interdite.

Par ailleurs, l'utilisateur s'engage à respecter les droits moraux de l'auteur, principalement le droit à l'intégrité de l'oeuvre et le droit de paternité et ce dans toute utilisation que l'utilisateur entreprend. Ainsi, à titre d'exemple, lorsqu'il reproduira un document par extrait ou dans son intégralité, l'utilisateur citera de manière complète les sources telles que mentionnées ci-dessus. Toute utilisation non explicitement autorisée ci-avant (telle que par exemple, la modification du document ou son résumé) nécessite l'autorisation préalable et expresse des auteurs ou de leurs ayants droit.

SMEM0029: Mémoire
Compact spectropolarimetry of auroral lights
Master Thesis

Garny Alexandre

Master in Space Sciences
Science Faculty



2020-2021

Contents

1	Introduction	4
1.1	Methodology	4
2	Auroras	6
2.1	Link with the atmospheric composition	7
2.2	Desexcitation process	8
2.3	Source of this excitation	9
2.4	Impact of space weather	10
3	Polarisation	12
3.1	Mathematics behind polarisation	13
3.2	Source of atmospheric polarisation	14
3.2.1	Rayleigh scattering	14
3.2.2	Mie scattering	15
3.2.3	Closing remark	16
3.3	Polarisation in the auroral lights	16
3.3.1	Previous observations	16
3.3.2	Unwanted polarisation source	18
4	Mathematical description of the polarisation	21
4.1	Formalism	21
4.1.1	Stokes parameters	21
4.1.2	Mueller formalism	23
4.1.3	Poincaré sphere	24
4.2	Noise and signal to noise ratio (SNR)	25
4.2.1	Poissonian noise	26
4.2.2	Gaussian noise	26
4.3	Visibility	26
5	Spectropolarimetry	27
5.1	Polarimetry	27
5.1.1	Classical measurement method	28
5.1.2	Concept of compact/static polarimetry	30
5.2	Birefringent material	31
5.3	Spectral part	32
5.4	Other current examples of spectropolarimeters	34
5.4.1	ZIMPOL	34
5.4.2	SO/PHI	36
5.4.3	SPEXone	37

6	Modus operandi of the instrument	39
6.1	First wedge	39
6.2	Second wedge	40
6.3	Third wedge	41
6.4	Analyser	42
6.5	Values for typical polarisation vectors	43
7	Simulations	49
7.1	Algorithm	49
7.1.1	Inverse Matrix technique	50
7.1.2	Signal fitting	51
7.2	Instrument precision	51
7.3	Simple signal	52
7.3.1	Without noise	52
7.3.2	Impact of perturbations on the expected precision . .	56
7.3.3	Main source of imprecision	63
7.4	"Realistic" signal	63
8	Possible instrument optimisation	65
8.1	Change in the pixel amount	65
8.2	Increasing spatial precision by splitting the output signal . .	66
9	Conclusion	69
	References	71

Acknowledgments

I would like first of all to thanks professor J.Loicq for accepting to supervise this work. I would also like to thanks Mr Vasilescu, his PhD student, that was always there when I had any question and greatly helped me develop the mathematical model of the instrument.

I would also like to thank my parents and my brother, who supported me trough these harder times.

1 Introduction

To everyone that had the chance to see one, auroras are fascinating night lights. But despite recent studies over the last decade, some of their properties remain uncertain due to their unstable nature. This is why we need a new type of instrument able to, if not add precision, offer a new way of studying auroras, and in our case, their polarisation in relation to their spectrum.

Polarisation analysis provides a way to extract information from the light we receive while still being compatible with imaging. For example, it is used in astronomy to study various astronomical phenomena, but it is also used in the medical domain, in defence, ...

The objective of this work is to see if it would be possible to adapt the spectropolarimeter instrument developed by Mr Vasilescu et al [1] to the study of auroral emissions, and if it would be more interesting than the current method. It was also a way to study the behaviour of the instrument when exposed to partially polarised light, rather than completely polarised light like studied before ([1]). As the instrument does not exist yet, all developments are theoretical and based on a mathematical model.

1.1 Methodology

To achieve this goal, we first presented the instruments used in previous aurora observation campaigns, their setup and theoretical precision, before trying to evaluate the precision of the new technique by looking at the impact of various imprecisions that can appear.

Reasons The study of polarisation in general can be a hard challenge, and the study of a phenomenon as fluctuating as the auroras can render this even trickier, as they are quite unstable. As so, the current methods, which require waiting for sometimes long integration periods, can give us false or imprecise results. The use of a different faster way to observe the polarisation of the auroras could help us get better results and improve their precision.

The reason to study the polarisation of a beam of light is that it can inform us of the properties of its source and/or on the medium it crossed to get to the observer. More precisely, the study of the aurora polarisation can help us study a proxy of the space weather and earth's magnetic field activity.

This also offers us another possibility to study ionospheric currents, even if there are other, and better, ways to do it.

The work will be divided into 9 chapters. The first chapters will be dedicated to the concept used in the study, before developing the work in itself.

In the second chapter, we will talk about the aurora phenomenon, its source and the impact of space weather.

In the third chapter, we will talk about polarisation, briefly talk about the most common natural sources and give a preview of the math behind it.

In the fourth chapter, we will talk about spectropolarimetry and specify the technique behind our work.

The fifth chapter gives a mathematical description of the instrument we used.

The sixth chapter talks about the concept behind our instrument and how it does work.

The seventh chapter is dedicated to the simulations, first the theory behind the algorithm, then the various step that we followed and the results obtained.

In the eighth chapter we will investigate ways of optimising the instrument for this usage.

And finally we have the conclusion.

2 Auroras

In this chapter, we will describe what auroras are and what their source process is.

First we have to set what is an aurora.

Auroras, also called "northern lights" in our regions, are very rapidly changing atmospheric luminous events, seemingly spontaneous, appearing in the sky of both arctic and antarctic circles. In the northern hemisphere they are called "Aurora Borealis" and in the southern hemisphere "Aurora Australis". They usually show green or less frequently red/pinkish colour, spread over large parts of the night sky and form at high altitude (over 100 km height, and up to 400 km).

They are quite frequent at latitudes higher than the polar circles but can be exceptionally seen in lower latitude regions during extreme solar events. I personally had the chance to see some during a trip to northern Sweden.



Figure 2.1: Auroral lights in the swedish sky

Most auroras are created by the radiative transition of atmospheric atoms and molecules, specifically Oxygen atoms and di-Nitrogen molecules in our case, as well as by Hydrogen and Helium in a lesser way. Those last ones (H and He) are rarely visible to the naked eye, and since we will only

focus on the transition in the visible domain we won't go over them. However we also have the case of some precipitating protons coming from space that can briefly couple with atmospheric electrons, form Hydrogen atoms and emit transition photons.

Be it caused by the first of the second type of source, we can say that auroras are essentially the visible part of the space weather impact on the earth's magnetosphere.

2.1 Link with the atmospheric composition

At the altitude of emission, the atmospheric composition isn't the same as near the ground. Essentially we can divide the atmosphere into two big parts: The homosphere (located roughly under 100 km), where the component repartition of the atmosphere remains constant, and the heterosphere, where the concentration of its components varies at different rates. This is why the main auroras we see are coming from the local main components of the atmosphere at their altitude of formation: mainly N_2 and O, and why the Hydrogen auroras are constrained under 100 km (the hydrogen concentration peaks at 90km before rapidly decreasing above 100 km).

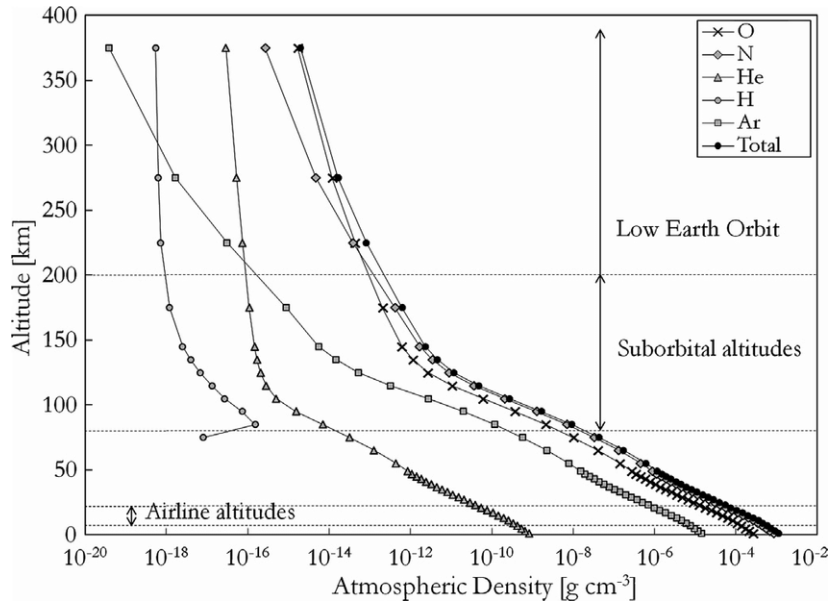


Figure 2.2: Atmospheric density ($g\ cm^{-3}$) and composition as a function of altitude (km) at solar minimum conditions determined using the NRLMSIS-00 atmospheric density model.[2]

For example the N_2^+ decay is associated with 427.8 and 391.4 nm wavelength photons, an altitude of roughly 100 km, and is caused by collision with charged particles (protons and electrons) coming from space. While the Oxygen is linked with \pm 630 nm wavelengths photons (630.03, 636.37 and 639.17 nm lines, each from 1D to 3P transition), that peaks around 210 km altitude, and 557.73 nm emissions, linked to the 1S to 1D transition and an altitude of 110 km, that can be caused by various sources: charged particles collision of course, but also daytime UV radiation coming from the sun.

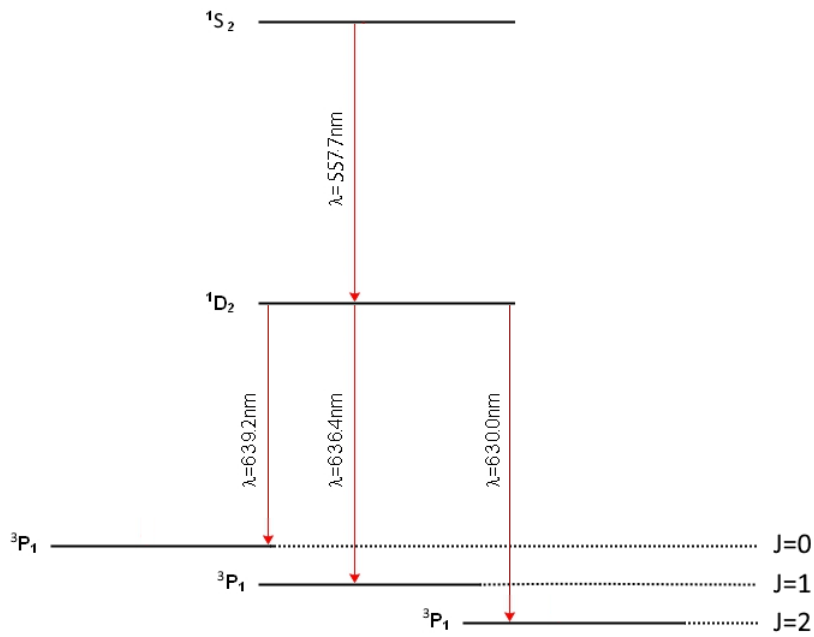


Figure 2.3: Atomic transitions of the O atom associated with auroras

2.2 Desexcitation process

The process of radiative spontaneous emission is a process during which an atom or a molecule lower its electronic energy level from an unstable or metastable position to a more stable one by releasing a photon of the same energy as the gap between the two levels. This process can be spontaneous, but can also be stimulated like in current laser sources.

Each probability of transition is described by an einstein coefficient. For example, if we consider two energy levels, and n_2 atoms in the unstable higher one, the evolution of the number of atoms in this higher energy state

if left undisturbed is described by the following equation:

$$\frac{dn_2}{dt} = -A_{21}n_2 \quad (2.1)$$

With A_{21} the Einstein coefficient (established experimentally and available on the NIST website [3]) associated with this transition. This gives us a law of exponential decrease of n_2 over time. It also gives us an estimation of the mean lifetime of an excited level, noted τ , expressed as:

$$\tau = \frac{1}{n_0} \int_{t=0}^{\text{inf}} t |dn_2| \quad (2.2)$$

$$\tau = \int_{t=0}^{\text{inf}} t A_{21} e^{-A_{21}t} dt = \frac{1}{A_{21}} \quad (2.3)$$

With n_0 the initial number of atoms in the high energy level at $t=0$.

The atom/molecule can also exchange energy with its neighbours by collision. If the medium density is sufficient, this becomes the main source of de-excitation and is why auroras do not appear at lower altitudes. But these collisional de-excitations play a less important role in the rarefied atmosphere where the auroras appear. One can easily verify this with a vacuum pump and a small potential generator.

The whole collision-desexcitation process can be synthesized as follow: An atmospheric particle X receive energy coming from the collision with trapped charged particles (here an electron), and is put in an unstable or metastable excited state X^* .



It then releases this excedent of energy to reach a more stable energy state by emitting a photon of the same energy.



The energy of this photon can be expressed as $E = h\nu_\gamma$, with h Planck's constant and ν_γ the frequency of the photon.

2.3 Source of this excitation

The main source of atmospheric atoms excitation during the night is the collision with charged particles trapped by the magnetosphere penetrating deep within the atmosphere.

Those particles initially come from the solar wind and more generally from

the interplanetary medium. Some of these charged particles are trapped by the geomagnetic field and remains within the magnetosphere. Their trajectory is somewhat convoluted, as they spiral around the magnetic field lines, bouncing back and forth between their mirror points. Their trajectory can lead them deeper within the earth's atmosphere when they approach a magnetic pole and its weaker field, leading to said collisions with the atmosphere components.

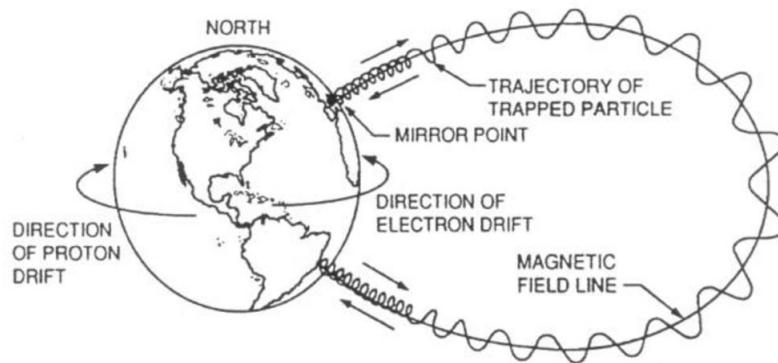


Figure 2.4: Representation of the composite motion of charged particles trapped in the Earth's magnetic field, credit:[4]

High auroral activities can be linked with storms/ high geomagnetic activity, that increase the number of particles reaching the earth. Indeed those events decrease the earth's magnetic field strength and increase the upper atmosphere's temperature, expanding it and allowing the trapped charged particle to penetrate deeper, hence the increased auroral activity.

2.4 Impact of space weather

What we call space weather is the result of the interactions between the earth's magnetosphere and the emissions of the sun (radiations, but also charged particles) having an impact on the earth and human activities. Those emissions are not uniform, and higher activity periods lead to perturbations of the earth's direct environment called storms.

Other than auroras, Storms can cause various disruptions, like electrical systems or weather perturbation. The scale of these is directly dependent on the ionospheric induced current and their cause, geomagnetic field perturbations.

The most known examples are the Canadian transformers meltdown in 1989, and telegraph lines destruction accompanied by operator electrocution during the biggest recorded solar storm in 1859, known as the Carrington Event.

3 Polarisation

In this chapter, we will describe the concept of polarisation and the main source that we could encounter. We will also talk about the previous observation campaigns that have been done to study auroral polarisation. Polarisation is a fundamental property of light. It is the expression of the orientation of the oscillation plane of the electric field in an electromagnetic wave.

The polarisation that we talk about in our case is a preferred direction of oscillation, indicated by an excess of photons polarised in a given direction. Since our eyes are not sensitive to the polarisation state of light, it is hard to realise all the polarised light present around us. For example, most of the reflected, transmitted and scattered light has a slightly induced polarisation. For reflections, it is because the light hit the reflective surface with an angle, and so the differently polarised components will not see the surface the same way. This is why polarised lenses can be used in fishing or photography to limit the reflection on the surface of the water. For the transmittance, it is linked to the properties of the material. This will induce a retardance, a modification of the polarisation state.

If the direction of polarisation does not change over time, the polarisation is said to be linear. On the contrary, if the polarisation plane changes over time, the polarisation is said to be elliptical, or circular (rotating clockwise or anti-clockwise) if the rotation of the plane is regular.

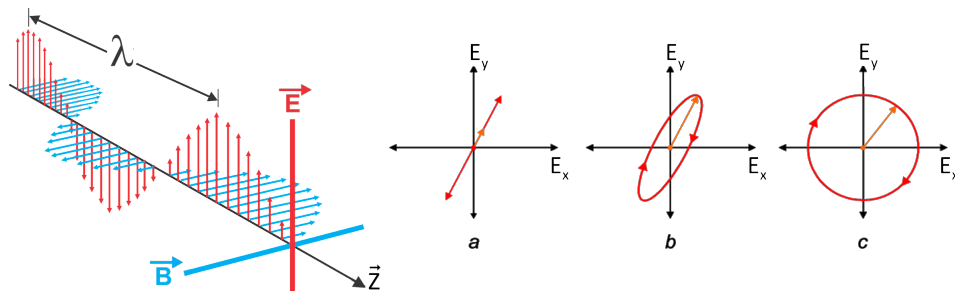


Figure 3.1: Polarisation states, linear (a), elliptical (b), right circular (c), credit:[5]

The way to measure polarisation will be developed in the next chapter.

3.1 Mathematics behind polarisation

A short reminder may be necessary. As long as we don't look at its interaction with matter, light can be considered as a pure transverse electromagnetic wave, with its electric and magnetic field oscillating in phase, perpendicularly relative to each other and to their displacement direction. The most commonly used reference frame place this direction of propagation on the z axis, and the electric and magnetic oscillations in the x - y plane. While there is no ambiguity regarding the z direction, the x and y axis are arbitrary fixed by the observer. The electric field part can be described as:

$$\vec{E}(z, t) = \vec{E}_x(z, t) + \vec{E}_y(z, t) \quad (3.1)$$

$$\vec{E}_x(z, t) = E_{0x} \cos(kz - \omega t) * \vec{e}_x \quad (3.2)$$

$$\vec{E}_y(z, t) = E_{0y} \cos(kz - \omega t + \epsilon) * \vec{e}_y \quad (3.3)$$

With k the wavenumber, ω the angular frequency, \vec{E}_{0x} the oscillation amplitude in the \vec{e}_x direction and \vec{E}_{0y} the one in the \vec{e}_y direction, and ϵ the phase difference between the two oscillations.

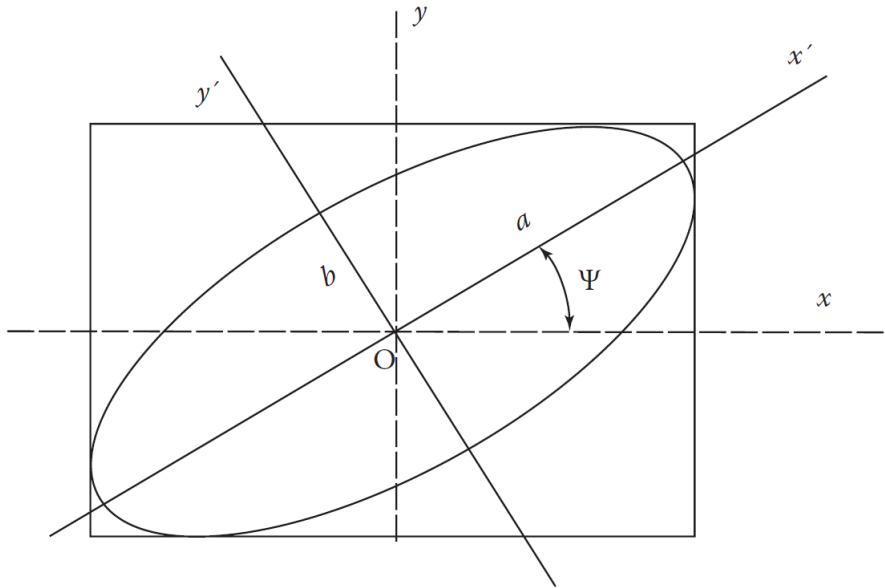


Figure 3.2: The polarisation ellipse rotated by ψ , credit:[6]

Getting back to Fig 3.1, one can easily see that the case (a), the case of a linear polarisation, corresponds to a value of ϵ equal to zero to a factor of π . The inclination angle ν of the polarisation in regard to the x axis would

then be given by the arctangent of the ratio $\frac{E_{0y}}{E_{0x}}$. This angle is called the auxiliary angle.

On the other extreme, if we have a value of ϵ that is equal to $\frac{\pi}{2}$ (once again to a factor of π) and a ratio $\frac{E_{0y}}{E_{0x}} = 1$, we find ourselves in the case (c), the case of a circular polarisation. The direction of rotation of the polarisation determines if we are in a right circular (clockwise rotation) or a left circular (anti-clockwise rotation) polarisation.

And in the other cases we have what is called an elliptical polarisation. In this case, there is no relation between the values of E_{0x} and E_{0y} , and the phase difference is arbitrary. It can be seen as a superposition of case a) and c). To describe properly the elliptical polarisation, we need to define the elliptical parameters. In general, the ellipse has the form

$$\frac{E_x^2(z, t)}{E_{0x}^2} + \frac{E_y^2(z, t)}{E_{0y}^2} - 2 \frac{E_x(z, t)}{E_{0x}} \frac{E_y(z, t)}{E_{0y}} \cos \epsilon = \sin^2 \epsilon \quad (3.4)$$

The equation describing the angle Ψ between the major axis of the projected ellipse and the x axis, called angle of rotation is given by

$$\tan 2\Psi = \frac{2E_{0x}E_{0y}\cos\epsilon}{E_{0x}^2 - E_{0y}^2} = (\tan 2\nu)\cos\epsilon \quad (3.5)$$

And finally the last parameter of interest is χ the angle of ellipticity, defined as:

$$\tan \chi = \frac{\pm b}{a} \quad \sin 2\chi = (\sin 2\nu)\sin \epsilon \quad (3.6)$$

With a the semi-major axis and b the semi-minor axis of the ellipse.

Particular cases of linear polarisation that will be important later:

- polarisation along the main axis x or y. In this case, we have either $E_{0x} = 0$ (polarisation along the y axis), or $E_{0y} = 0$ (polarisation along the x axis).
- polarisation along a diagonal. In this case, $E_{0x} = \pm E_{0y}$, and the angle of the polarisation plane relative to the x axis is 45° or 135° .

3.2 Source of atmospheric polarisation

3.2.1 Rayleigh scattering

Main source of the atmospheric contribution to polarisation, the Rayleigh scattering appears when light encounters very small particles, way smaller than its wavelength. It typically appears when the light crosses gas, but can be seen with some transparent liquid and solid. The particle (be it atomic or molecular in nature) begins to oscillate with the electric part of the incident lightwave and emits with the same frequency. The phenomenon gets stronger as we get close to the resonance wavelength, and the scattering

efficiency is proportional to the fourth power of the frequency of the incident light.

The re-emission is not uniform, it can only occur in a plane transverse to the

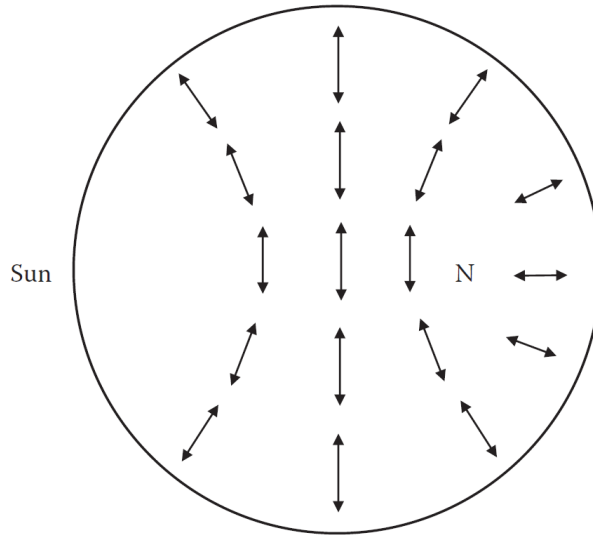


Figure 3.3: Polarization pattern of the sky when the sun is at the horizon. N indicates the neutral point of Arago (the point of no polarisation, in the anti solar direction). credit:[6]

incident light, and thus create a polarisation pattern in the light observed after the medium.

One can represent the polarisation of the visible sky as in Fig 3.3. We see that there is no polarisation in the sun's direction, nor in the one of the Arago neutral point, and that the maximum of polarisation is located at 90° from the sun. This polarisation pattern can be observed in the sun's light, and in the moonlight, despite being weaker. This will come back in a later chapter.

3.2.2 Mie scattering

Another big source of atmospheric polarisation, the Mie scattering appears when light encounter particles bigger than its wavelength, for example water droplets, dust or, more interesting in our case, ice crystals.

It can be seen by the formation of a "halo" around the light source when it appears. The forward direction of scattering is favoured, by comparison with the Rayleigh scattering.

At this scale, the shape of the particle is important, as it creates asymmetries in the scattered light pattern and its polarisation. To describe these asymmetries, one can define what is called the shape parameter, called x , so

that:

$$x = \frac{\pi d}{\lambda} \quad (3.7)$$

With d the diameter of the particle and λ the wavelength of the incident photon. We know that when the value of x gets small, the Rayleigh scattering is dominant, but as the value of x increase, the degree of polarisation repartition will change a lot from x to x , even allowing the apparition of radial polarisation relatively to the source. The mathematical description of the Mie scattering can be very complex in its pure form, so the numerical approach tends to be preferred in most of the case.

3.2.3 Closing remark

It is useful to remark that the polarisation described here are all linear, the apparition of circular polarising effect being more linked to the presence of organic compounds and their chiral properties or to multiple scattering processes. We won't talk about those as they do not take a role in the studied phenomenon, even if our instrument can detect them.

3.3 Polarisation in the auroral lights

3.3.1 Previous observations

The process of polarisation in the auroras has already been studied from the ground several times in the past, with campaigns during the 50's. These met an early end as it was initially thought that the polarisation of auroral light was impossible due to the source process they rely on.

These study started again more recently under the impulse of Lilensten and his team. They realised several observation campaigns (in 2012[7], 2015[8], 2016[9] and 2019[10]) as well as M.Barthelemy did in 2018([11]).

Used instrument

For these observations, they used an instrument called the SPP, or "spectro-photo-polarimeter" ([7], [8] and [9]), then the "premier cru" ([11]) and finally the "petit Cru" ([10]). All of which are spectrum targeted polarimeters. The SPP use the rotating polariser technique to study polarisation, and filters to isolate the desired wavelength. This polarimetry technique and its differences with the one studied in this paper will be described in a following chapter.

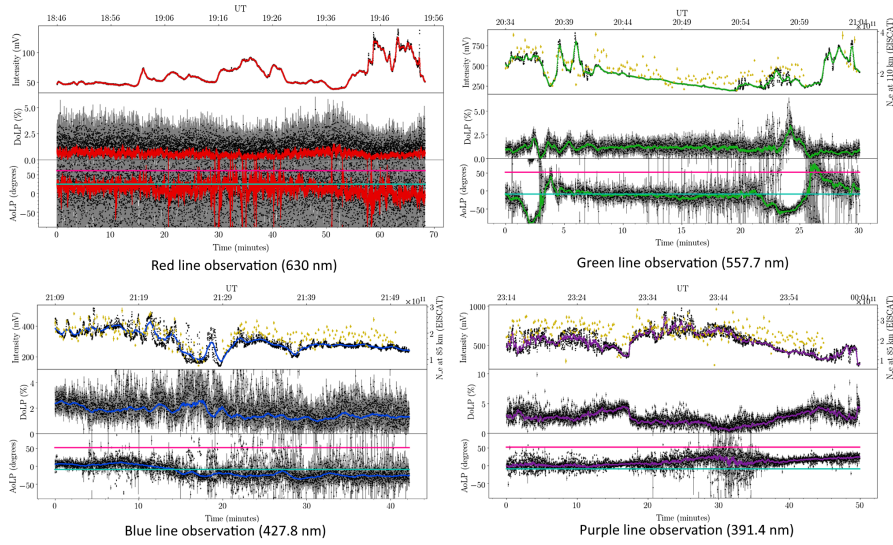


Figure 3.4: Previous observations in four wavelength. Each graph shows the Intensity, the linear polarisation degree and the angle of polarisation in function of the time. credit:[10]

Results

The observations were realised at different wavelengths as they each correspond to different events, and are associated to specific altitudes as said in chapter 2. The results show that each of those events can be differently polarised and that those DoLP (Degree of Linear Polarisation) are not linked. This was to be expected, as they are not correlated nor do take place at the same height.

The degree of linear polarisation measured (from 0 to 8% for the O red line, 0 to 3% for the O green light, currently thought to be non-polarisable due to its source process [12], 1 to 3% for the blue N_2^+ line, and 1 to 5% for the purple N_2^+ line) showed dependence with the orientation of the instrument, with a maximum when the instrument is aligned with the overhead magnetic field direction, as well as with the intensity of the auroral emission. Another observation was that the DoLP tends to decrease as the intensity increases due to the higher collision probability between atmospheric particles.

But as with all earth-based observation, the results are localised and not reproducible everywhere (due to the limited zones where auroras appear they are limited to the polar emerged lands). The use of space-based instruments could allow a more global approach and measurements to be independent of the crustal field.

These observations showed that auroral light could be polarised as the result of different phenomena.

The main one is the source process, which is not always isotropic. This is linked with the fact that, as said in the previous chapter, auroral lights are caused by collisions between the trapped solar particle precipitation and the atmosphere, and that these particles are collimated with the magnetic field lines, resulting in an anisotropic process.

The reality is that the possibility of direct polarisation from the aurora cannot be confirmed nor denied, and that the physics responsible for the nightglow polarisation is still not perfectly understood.

3.3.2 Unwanted polarisation source

Artificial

Just like any night observation, the previous observations have shown that ground light sources can perturb the result of experiments, as their light is scattered to the instrument and polarised by Rayleigh scattering.

Another big source of pollution is the internal reflections and irregularities in the instrument. These perturbations can for example be caused by the imprecisions in the wedge manufacture, irregularities at their meeting point and surfaces.

Natural

But other natural phenomena can also change the values that we measure. For example, let us study the impact of the Faraday rotation appearing in the ionosphere. The Faraday rotation in itself does not create polarisation, but modifies the linear polarisation state of the light.

The Faraday rotation, or magneto-optical effect, is a phenomenon appearing when polarised light crosses a dielectric material along the magnetic field direction. It can be understood very intuitively by imagining the charged particle following the electric field of the light being submitted to the magnetic force, forcing the oscillation plane to rotate with them. It follows that the rotation is proportional to the field intensity and the length of its path within said magnetic field. The resulting rotation angle θ can be expressed as:

$$\theta = \nu_V(\lambda) \vec{B}d \quad (3.8)$$

With ν_V a constant called Verdet's constant, linked with the light's wavelength, B the magnetic field strength (expressed in Tesla) and d the crossed length (in meter). ν_V is typically very small, but depends on the properties of the material.

The rotation direction do not depends if you travel the same way as the field or in opposite direction.

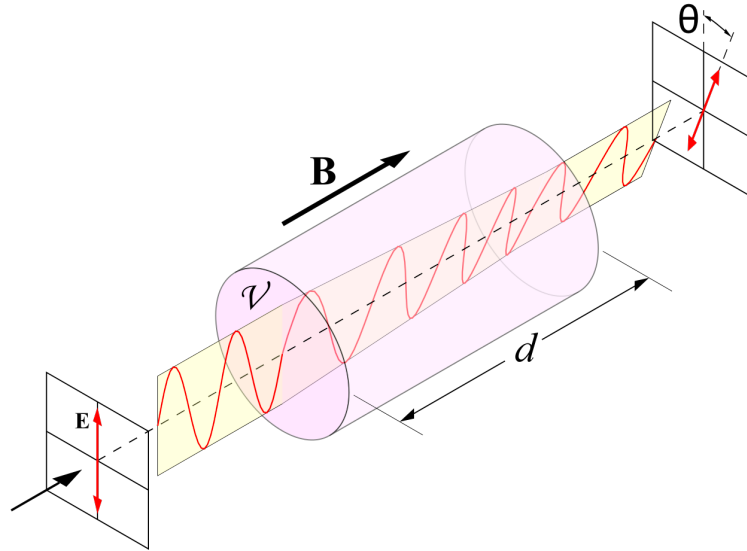


Figure 3.5: Faraday rotation of an incident linear polarisation. credit: thorlabs.com

In our case the ionosphere can cause this type of effect due to the presence of free electrons. The incoming linearly polarised light is split into two circular polarised components having slightly different propagation speeds. Those two components recombine at the end of the ionised medium, but with a modified polarisation angle. The outgoing polarisation is shifted by an angle of $\Omega = \frac{2.365 \cdot 10^4}{f^2} * VTEC * \frac{1}{\cos \gamma} * B_{\parallel}$ [10], with f the light frequency (in GHz), $VTEC$ the Vertical Total Electron Content (in TEC Unit), $\frac{1}{\cos \gamma}$ the factor to go from VETC to TEC, γ the apex angle and B_{\parallel} the the mean geomagnetic field in the crossed part of the ionosphere parallel to the observed direction (in Tesla).

If we know roughly the initial polarisation direction and can measure the final one, it can give us information about the state of the ionosphere. However, it seems this effect is negligible in the earth's environment, at least for the wavelength studied here since its effect is not observed for frequencies higher than those of radio waves.

A similar effect, called The Kerr effect, can be observed in regions of high electric fields.

The previous measurements have also shown that the polarisation nearly disappears during the day, as the dominant process of excitation becomes the EUV coming from the sun. These emissions are then subjected to rayleigh scattering and polarised accordingly. As previously said, this is also the case with moonlight, so periods without lunar presence have to be preferred for good observations.

4 Mathematical description of the polarisation

In this chapter, we describe the formalism that we used to describe the polarisation, and the main source of imprecision that we will encounter: noise. Noise being a general term regrouping all the unwanted sources of signal appearing on our detector. The formalism description will spread over this chapter and the next, this one serving more to set up the basis.

Since there was no already built instrument to work with, the entire work was made in simulations.

4.1 Formalism

Previously we described the polarisation state of the incident light using the polarisation ellipse (section 3.1), however, despite being quite intuitive, this representation is not that convenient: first of all the period of rotation of the polarisation plane is generally of the order of 10^{-15} s, so it is impossible to measure directly, moreover, this representation does not account for partially polarised light, which limits its use to describe most of the encountered situations. Partially polarised meaning that the light will only show a small excess of polarisation in one direction. This ellipse has thus to be considered as an idealisation, and another representation was needed. To allow us to study and make simulations of the polarisation, we will then use the Stokes and Mueller formalism.

4.1.1 Stokes parameters

In this approach, way more convenient for simulations, we represent the polarisation degrees as a set of four Stokes polarisation parameters. One can write them down as:

$$S_0 = E_{0x}^2 + E_{0y}^2 \quad (4.1)$$

$$S_1 = E_{0x}^2 - E_{0y}^2 \quad (4.2)$$

$$S_2 = 2E_{0x}E_{0y}\cos(\epsilon) \quad (4.3)$$

$$S_3 = 2E_{0x}E_{0y}\sin(\epsilon) \quad (4.4)$$

In this notation, S_0 (called I afterwards) is the total intensity, S_1 (called Q) is the linear polarisation along the classical X and Y axis, with X along the horizontal plane of the instrument, and Y along its vertical, S_2 (called

U) is the linear polarisation along the $\pm 45^\circ$ axis and S_3 (called V) is the circular polarisation (right or left). E_x and E_y are the orthogonal electric field component amplitude and ϵ is the phase difference between them. It can be shown that they obey to the relation.

$$S_0^2 \geq S_1^2 + S_2^2 + S_3^2 \quad (4.5)$$

There is equality only if the light is completely polarised. In other cases we can see the partially polarised light as a superposition of two components: one completely polarised ($I_{polarised}$) and one not ($I_{unpolarised}$). The intensity then becomes

$$I^2 = I_p^2 + I_u^2 \quad \text{With} \quad I_p^2 = S_1^2 + S_2^2 + S_3^2 \quad (4.6)$$

It also allows us to write the degree of polarisation p as:

$$p = \frac{\sqrt{S_1^2 + S_2^2 + S_3^2}}{I} \quad (4.7)$$

With the value of p comprised between 0 (no polarisation) and 1 (fully polarised). In our case since the incident light polarisation is purely linear, we can pose $V=0$ and define the degree of linear polarisation (DoLP) as:

$$p_{lin} = \frac{\sqrt{S_1^2 + S_2^2}}{I} \quad (4.8)$$

and the angle of linear polarisation (AoLP) θ

$$\cos(2\theta) = \frac{\frac{S_1}{S_0}}{p_{lin}} \quad (4.9)$$

$$\sin(2\theta) = \frac{\frac{S_2}{S_0}}{p_{lin}} \quad (4.10)$$

$$\theta = \frac{1}{2} \text{atan}\left(\frac{S_2}{S_1}\right) \quad (4.11)$$

Having now properly defined the Stokes parameters, we can go back to the polarisation parameters defined previously in chapter 4, and express them in our new representation.

The angle of rotation Ψ can now be written as:

$$\tan 2\Psi = \frac{2E_{0x}E_{0y}\cos\epsilon}{E_{0x}^2 - E_{0y}^2} = \frac{S_2}{S_1} \quad (4.12)$$

Similarly, one can express the angle of ellipticity χ as

$$\sin 2\chi = \frac{2E_{0x}E_{0y}\sin\epsilon}{E_{0x}^2 + E_{0y}^2} = \frac{S_3}{S_0} \quad (4.13)$$

For convenience the Stokes parameters can be represented as the elements of a length four vector, called the Stokes vector.

$$S = \begin{pmatrix} I = S_0 \\ Q = S_1 \\ U = S_2 \\ V = S_3 \end{pmatrix} \quad (4.14)$$

This notation will be used from now on.

4.1.2 Mueller formalism

To represent the impact of the instrument optical elements on the polarisation state of the crossing light, we will use the Mueller calculus. Using the Stokes parameters representation, this consist of associating every optical element with a transformation matrix, called a Mueller matrix. Obtaining the polarisation state at the exit of the system becomes a simple matrix product.

We will consider an incoming beam of light described by the Stokes vector $S = (I, Q, U, V)$ (which is written vertically), and an instrumental Mueller matrix M written as.

$$M = \begin{pmatrix} m_{00} & m_{01} & m_{02} & m_{03} \\ m_{10} & m_{11} & m_{12} & m_{13} \\ m_{20} & m_{21} & m_{22} & m_{23} \\ m_{30} & m_{31} & m_{32} & m_{33} \end{pmatrix} \quad (4.15)$$

To express the outgoing beam, we will use the notation \tilde{S} , that can be expressed as $\tilde{S} = M * S$, or

$$\tilde{I} = m_{00}I + m_{01}Q + m_{02}U + m_{03}V \quad (4.16)$$

$$\tilde{Q} = m_{10}I + m_{11}Q + m_{12}U + m_{13}V \quad (4.17)$$

$$\tilde{U} = m_{20}I + m_{21}Q + m_{22}U + m_{23}V \quad (4.18)$$

$$\tilde{V} = m_{30}I + m_{31}Q + m_{32}U + m_{33}V \quad (4.19)$$

The Mueller matrix of the whole instrument is then the product of its different element's matrices. One can synthesise the whole system as

$$S_{out} = \begin{pmatrix} I_{out} \\ Q_{out} \\ U_{out} \\ V_{out} \end{pmatrix} = M_n * M_{n-1} * \dots * M_1 * \begin{pmatrix} I_{in} \\ Q_{in} \\ U_{in} \\ V_{in} \end{pmatrix} \quad (4.20)$$

With n the number of elements encountered by the beam and the index being their position in the optical setup (n being the closest to the detector). As we are using matrix multiplication, the order in which the Mueller matrices are set up is very important if we want to achieve correct results.

The problem is now to find the values of the elements composing our system. Luckily this has already been done in a previous work [1]. The values are given in the following chapter.

4.1.3 Poincaré sphere

A visual and convenient way of representing the Stokes vector is by placing it in a three dimensional reference frame using its U, V and Q parameters as x, y and z coordinates. The radius is thus given by the intensity of the polarised part of the light. This sphere is called the observable polarisation sphere.

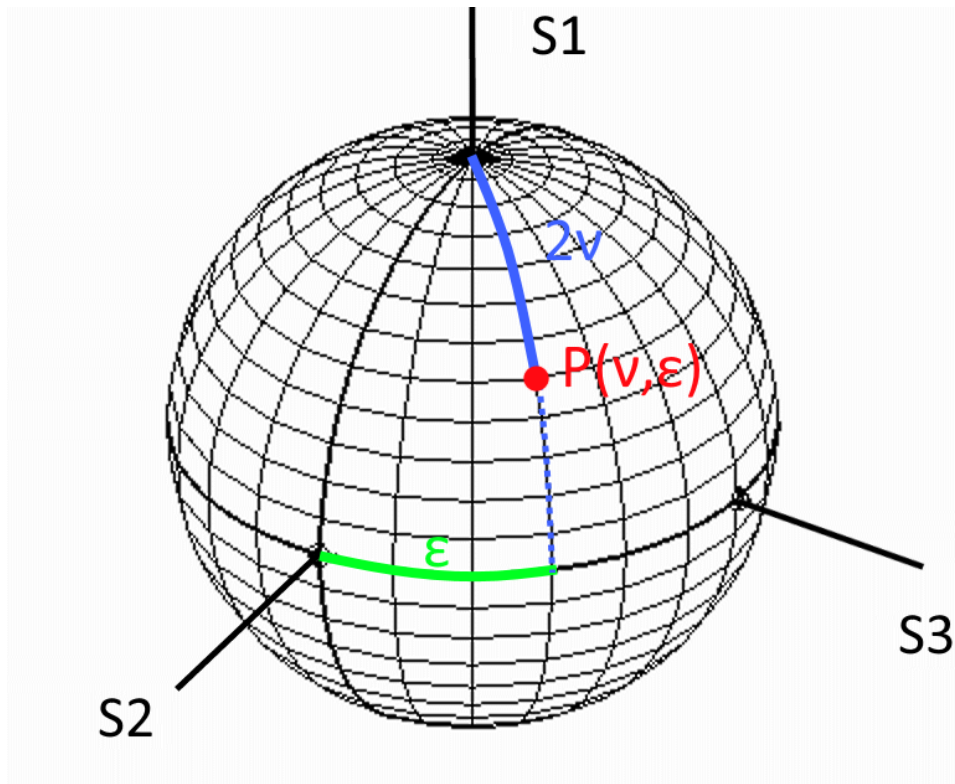


Figure 4.1: Polarisation P represented over the Poincaré/Observable Polarisation sphere. credit:[13]

tion sphere and allows us to represent the transformations undergone by the beam as it crosses the system.

We can now write the Stokes vector as:

$$S = \begin{pmatrix} 1 \\ p \cos 2\nu \\ p \sin 2\nu \cos 2\epsilon \\ p \sin 2\nu \sin 2\epsilon \end{pmatrix} \quad (4.21)$$

With p the polarisation degree, ν the inclination angle and ϵ the phase difference between the E_x and E_y component of the associated point $P(\nu, \epsilon)$'s polarisation, used as spherical coordinates.

The output Stokes vector is obtained by multiplying it by the Mueller matrix of the system. This will be developed in detail during the next chapter. For example, here is the representation of an output Stokes vector associated with a general polariser (linear diattenuator) of angle θ :

$$\tilde{S} = \frac{1}{2}[S_0 + S_1 \cos 2\theta + S_2 \sin 2\theta] \begin{pmatrix} 1 \\ p \cos 2\theta \\ p \sin 2\theta \\ 0 \end{pmatrix} = \begin{pmatrix} 1 \\ p \cos 2\tilde{\nu} \\ p \sin 2\tilde{\nu} \cos 2\tilde{\epsilon} \\ p \sin 2\tilde{\nu} \sin 2\tilde{\epsilon} \end{pmatrix} \quad (4.22)$$

We see that the outgoing polarisation state is only function of said θ angle, the initial parameters only serving as amplitude factor.

Similarly we can always represent the Stokes parameters of the light coming out of a retarder of fast axis α in function of the incoming Stokes parameters.

By studying the $P(\tilde{\nu}, \tilde{\epsilon})$ associated with different values of α and θ , we can see that those points will describe a circle inscribed on the surface of the sphere. The axis around which those circles will be described doesn't depend on the modified parameter: by modifying either α or θ the point P will rotate around the S_3 axis.

4.2 Noise and signal to noise ratio (SNR)

Signal noise is an unwanted perturbation of the output signal. It can be created by various phenomena affecting the detector.

The SNR is like its name implies the ratio between the signal and the noise. It can help us evaluate the quality of our measurement.

A general expression of the SNR can be written as

$$SNR = \left(\frac{1}{I} \sqrt{N_s^2 + N_{DC}^2 + N_{read}^2} \right)^{-1} \quad (4.23)$$

with N_s the noise associated with the signal, N_{DC} the noise associated with the dark (or thermal) noise, and finally like its name implies N_{read} is the noise associated with the reading error on the detector and is intrinsic to the detector.

In our case the noise associated with the instrument can be described using two main types of noise distribution: Gaussian and Poisson, associated with different noise sources.

4.2.1 Poissonian noise

The Poissonian noise (also called shot noise) is the noise created by the statistical nature of the light at low exposure and is proportional to the square root of the signal. It is called Poissonian noise because it follows a Poisson distribution.

You cannot lower it, but by having a stronger signal you can mitigate its impact on your final results.

4.2.2 Gaussian noise

The Gaussian noise is linked to the detector thermal noise and appear regardless of the incoming signal. As its name implies it follows a normal distribution. This type of noise can be reduced by lowering the detector temperature, but is a nuisance for precise and/or low signal measurements. In our case, we had to fix values based on known detector properties.

4.3 Visibility

Another way to estimate the quality of the output signal is by giving a value of its contrast. This value is called the visibility and is a dimensionless number given by the following equation:

$$V = \frac{I_{max} - I_{min}}{I_{max} + I_{min}} \quad (4.24)$$

With I_{max} and I_{min} the maximum and the minimum value of the output signal respectively. Those values are the ones picked up by the detector's pixels, meaning that they will be impacted by every imprecision affecting said pixels.

5 Spectropolarimetry

In this chapter, we describe the concept of spectropolarimetry using the formalism presented in the previous chapter. We also present other spectropolarimetric instruments.

Spectropolarimetry is the simultaneous study of spectrum (spectrometry) and polarisation (polarimetry) of the received light. This simultaneous study of both values allows to differentiate the polarimetric effects on each wavelength and their associated source process. In our case it allows us to study each type of auroras independently without pollution coming from one to another.

5.1 Polarimetry

Polarimetry is the study of polarisation. It is classically done by using a modulator followed by a polariser. This combination of optical element transforms a polarisation into an intensity variation. This conversion to intensity variation is needed because typical detectors (like CMOS and CCD sensors, or even the human eye) are intensity sensitive, but not polarisation sensitive.

Modulator Modulators, also called linear retarder, are polarising elements changing the phase of the optical beam. They induce a shift ϕ between the orthogonal field components. The general Mueller matrix associated with an ideal retarder of fast axis α° is

$$M = \begin{pmatrix} 1 & 0 & 0 & 0 \\ 0 & \cos^2 2\alpha + \sin^2 2\alpha \cos \phi & (1 - \cos \phi) \cos 2\alpha \sin 2\alpha & \sin 2\alpha \sin \phi \\ 0 & (1 - \cos \phi) \cos 2\alpha \sin 2\alpha & \cos \phi \cos^2 2\alpha + \sin^2 2\alpha & -\cos 2\alpha \sin \phi \\ 0 & -\sin 2\alpha \sin \phi & \cos 2\alpha \sin \phi & \cos \phi \end{pmatrix} \quad (5.1)$$

with ϕ the induced phase difference between the orthogonal components of the incident beam. The modulator is usually a fixed retarder (generally a quarter wave plate, meaning that the induced phase difference ϕ is $\pi/2$). For a typical ideal modulator with a fast axis $\alpha = 0^\circ$, the outgoing Stokes

vector is thus expressed as:

$$\tilde{S} = \begin{pmatrix} I_0 \\ Q_0 \\ U_0 \cos\phi + V_0 \sin\phi \\ -U_0 \sin\phi + V_0 \cos\phi \end{pmatrix} \quad (5.2)$$

As we can see, the retarder can only couple two polarisation states, this will be important later. Indeed, we can always orient our reference frame in a way to make the fast axis be in the $\alpha = 0^\circ$ direction, and make the previous expression reappear. One should know that in reality, as with any optical element, a little part of the intensity is lost, either absorbed by the element or reflected away, but it will not be considered here.

Analyser The second element, the analyser, is the piece that will transform the polarisation variation into an intensity variation. The Mueller matrix of an analyser of orientation θ is given by:

$$M_A(\theta) = \frac{1}{2} \begin{pmatrix} 1 & \cos 2\theta & \sin 2\theta & 0 \\ \cos 2\theta & \cos^2 2\theta & \cos 2\theta \sin 2\theta & 0 \\ \sin 2\theta & \cos 2\theta \sin 2\theta & \sin^2 2\theta & 0 \\ 0 & 0 & 0 & 0 \end{pmatrix} \quad (5.3)$$

with θ the angle between the transmission axis and the positive x axis. In the future we shall use the notation $c = \cos 2\theta$ and $s = \sin 2\theta$ for simplicity. A classical intensity output can then be expressed as $I_{out} = \alpha_{abs} I_{in} + \beta Q_{in} + \gamma U_{in} + \zeta V_{in}$, with α_{abs} being the absorption/intensity loss due to the system, and the other terms depending on the properties of the system. If those values are constants, we do not have enough equations to solve our unknowns and the degeneracy of the system cannot be lifted.

This issue can be solved by changing the orientation of one element relative to the other, typically by rotating it.

We see that the value of the outgoing intensity does not depend on the value of the circular polarisation. However, due to the presence of the modulator, one can extract the value of said circular polarisation from the values of the coupled linear polarisation term.

5.1.1 Classical measurement method

To study the three polarisation terms of the Stokes vector, a variation of the modulation is needed. It is classically done by using a rotating analyser, or by separating the two orthogonally polarised components of the light (ordinary and extraordinary) like the instrument used in the previous

observations:

The instrument they used, called SPP in its first iteration (in 2012[7], 2015[8] and 2016[9]) and "Petit Cru" in its latest (2019 campaign,[10]), is made off a telescope on which we put a rotating polariser followed by a spectrometer. The "Petit cru" was specialised to observe the four wavelengths described previously, while the SPP was focused on the observation of the 630 nm lines.

On the basis of this setup, we can obtain the system's mueller matrix, the one associated with a rotating polariser:

$$M_A(\theta(t)) = \frac{1}{2} \begin{pmatrix} 1 & \cos 2\theta(t) & \sin 2\theta(t) & 0 \\ \cos 2\theta(t) & \cos^2 2\theta(t) & \cos 2\theta(t) \sin 2\theta(t) & 0 \\ \sin 2\theta(t) & \cos 2\theta(t) \sin 2\theta(t) & \sin^2 2\theta(t) & 0 \\ 0 & 0 & 0 & 0 \end{pmatrix} \quad (5.4)$$

SPP's detector was only able to take measurements every 20th of a second and, combined with a polariser angular frequency of 90° per second, could reach a precision of $\Delta\theta = \pm 2.25^\circ$. Petit Cru used a more recent high speed detector able to take up to 1000 measurements per second and a tunable rotation speed polariser, able to go between 180 and 720° per second (the latter being the one used to allow fast measurements). Meaning the theoretical precision reach by the system is $\Delta\theta = \pm 0.36^\circ$.

Ultimately the precision is given by the output intensity variation, we thus have a precision that depends on $\frac{1}{2}\cos 2\theta$ for the S_1 parameter and $\frac{1}{2}\sin 2\theta$ for the S_2 parameter, meaning a precision that depends on the time of measurements as a variation of θ do not induce the same variation if it is made near $\theta = 0$ or $\theta = \pi/2$. The maximum imprecision is reached around $\theta = \pi/4$ and is the order of $\Delta I = \pm 0.055(S_1 + S_2)$ for SPP and $\Delta I = \pm 0.009(S_1 + S_2)$ for Petit Cru.

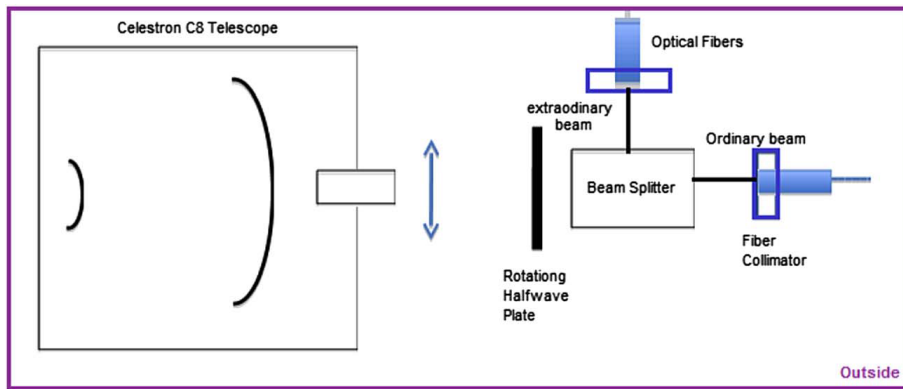


Figure 5.1: Schematic view of the premier cru polarimetry section, credit:[11]

The setup used by "premier cru" during the intermediary campaign of 2018[11] was different: After the telescope was placed a modulator with 4 possible orientations then a polarizing beam splitter cube that separated ordinary and extraordinary parts of the incident beam.

By changing the modulator orientation, we can scan over various values of α , and study the pattern on the different output intensity and extract the circular polarisation from it.

We can see that the polarisation analysis is conducted as early as possible. This is because it offers more protection against the unwanted polarisation induced by the instrument's optic.

5.1.2 Concept of compact/static polarimetry

By using a pair of birefringent prisms to spread the polarisation information spatially, one can study the light's polarisation without the use of moving parts. This technique is called compact spectropolarimetry, and is developed in a 2012 article from W.Sparks [14].

In the article, they present a method of polarimetry needing no moving

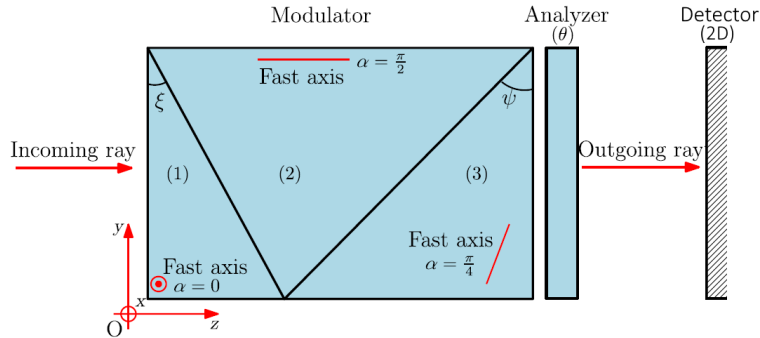


Figure 5.2: General representation of the compact polarimeter design proposed by Sparks. credit: [15]

parts while achieving high sensitivity. The main advantage of this configuration is that it allows us to study all the polarisation states simultaneously. The only limit becomes the resolution of the detector. The downside is a lower output intensity, and thus a higher SNR or integration time, as we are splitting the incident light rather than just observing the general intensity.

The design consist of a modulator, made out of two birefringent wedges having their fast axis oriented at 45° from each other and one not affecting the polarisation state of the light between them, followed by a classical analyser. The first wedge has its fast axis oriented at 0° relatively to the horizontal (x axis), and an apex angle ξ . The second wedge has its fast axis oriented along the ray progression direction (z) in a way to not modify the polarisation state of the light. Its role is to fill the gap between the two other wedges, limit the medium change effects by removing two wedge-air interfaces and add in solidity. The last wedge has its fast axis forming a 45° with the x axis, and an apex angle of Ψ . In our case, we took $\xi = 2.6^\circ$ and $\Psi = 1.6^\circ$, and an orientation of the analyser of $\theta = 50.6^\circ$. Two prisms are needed to lift the degeneracy on the linear components of the polarisation as shown in section 4.1. Indeed one prism can only allow the study of one linear polarisation type, as indicated by precedent studies ([14], [15]). Our resolution is thus independent of our detector measurement speed, it now relies on its pixel size. In our case, we have considered a detector composed of 1300 pixels each measuring 10^{-5} meter. However we still need to introduce some notions before calculating the impact of our system on the Stokes parameters and its precision.

This compactness and robustness can be a major advantage in demanding usage, for example in space, where the use of moving parts represent a liability.

5.2 Birefringent material

A birefringent material is a material showing different behaviour according to the polarisation state, effectively its refractive index will change with the incoming light direction and its polarisation orientation relative to its own optical axis, this property is called anisotropy as the material do not react the same way when observed from different directions. An example of naturally appearing birefringent material is quartz. It is the angle between this optical axis and the incoming light polarisation axis that will dictate the light behaviour inside the material. For example in the second wedge of our instrument (5.2), the optical axis is aligned with the light progression direction and so the polarisation state is not modified. However if the wedge optical axis and the light polarisation direction are not aligned, like the first and third wedge of the instrument, the path of the different polarisation states will differ, and we will see the appearance of a retardance proportional to the angle of this misalignment. A retardance is a variation of ϕ , the phase difference between the ordinary and extraordinary ray. As this variation depends on the path length, we can vary this length to study polarisation states, this is what is done by the instrument. We also align

the wedge optical axis with the horizontal and diagonal polarisation state respectively to allow Q and U analysis.

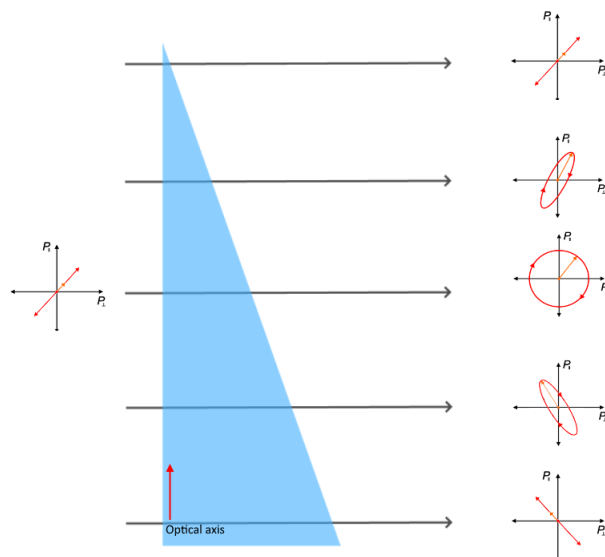


Figure 5.3: Schematic representation of the impact of the birefringent wedge on an incoming diagonal polarisation. The retardance increases with the wedge width.

Here we can observe the variation of the Q polarisation parameter (diagonal polarisation) as we move along the vertical axis. We see that there is a transfer from this diagonal polarisation to the circular polarisation as the retardance increase. Starting from the point where the light crosses without modification (thinner part of the wedge), we reach a width that induces a quarter-wave retardance, and all the light is converted to circular polarisation. Then we reach the point of half-wave retardance and we see that the initial polarisation has been rotated by 90° after the wedge. We will see this phenomenon more clearly in the sixth chapter.

In our case we consider the lens to be made out of MgF_2 , as chosen in the previous work [15] and will do our calculations accordingly.

5.3 Spectral part

The study of the spectrum is classically done by splitting the light into its different wavelength components either by making the light cross a prism

(made out of wavelength sensitive refraction indices material), or by reflecting on a diffraction grating (that uses the interference due to the different light path length to isolate wavelengths).

For example here is the design of a Czerny Turner spectrometer:

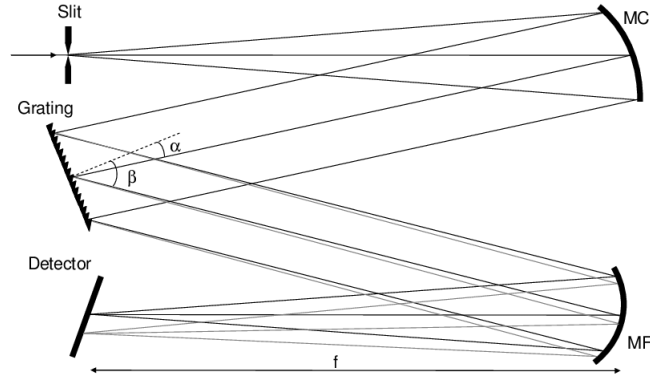


Figure 5.4: Classical Czerny-Turner spectrometer design, with MC the spherical collimating mirror, MF the spherical focusing mirror, f the effective focal length, and a grating with angles of incidence α and diffraction β . credit:[16]

This type of spectrometer is a standard design used in various domains.

In our case we will study the light spectrum and polarisation simultaneously. To achieve this, we simply put a spectrometer after the setup shown in 5.2 to disperse the spectrum orthogonally to the polarisation, and end up with one "spectral" direction and one "polarisation" direction. Like what is done in the 2012 Sparks's paper [14].

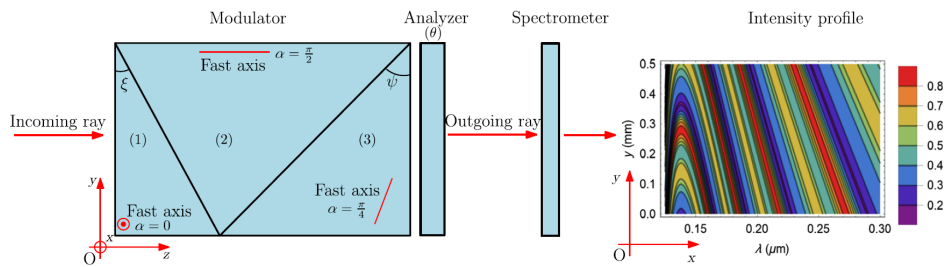


Figure 5.5: Design of the complete spectropolarimetry instrument developed by B.Vasilescu et al, credit [15]

As we only look at specific wavelength, the expected output would be a series of broadened lines around the desexcitation bands, as well as light pollution at different wavelength.

The choice of the birefringent prism material influences the spectrum that can be studied by the instrument via its transparency windows and its refraction indices.

5.4 Other current examples of spectropolarimeters

5.4.1 ZIMPOL

The ZIMPOL (Zürich IMaging POLarimeter) is part of the SPHERE instrument of the VLT. It was initially made to study the sun polarisation, but is now used to study nearby star's light linear polarisation for the research of big exoplanets orbiting them after proving to be using an extremely sensitive technique for polarization measurement. It was installed in 2014 and is now usable by the researcher community.

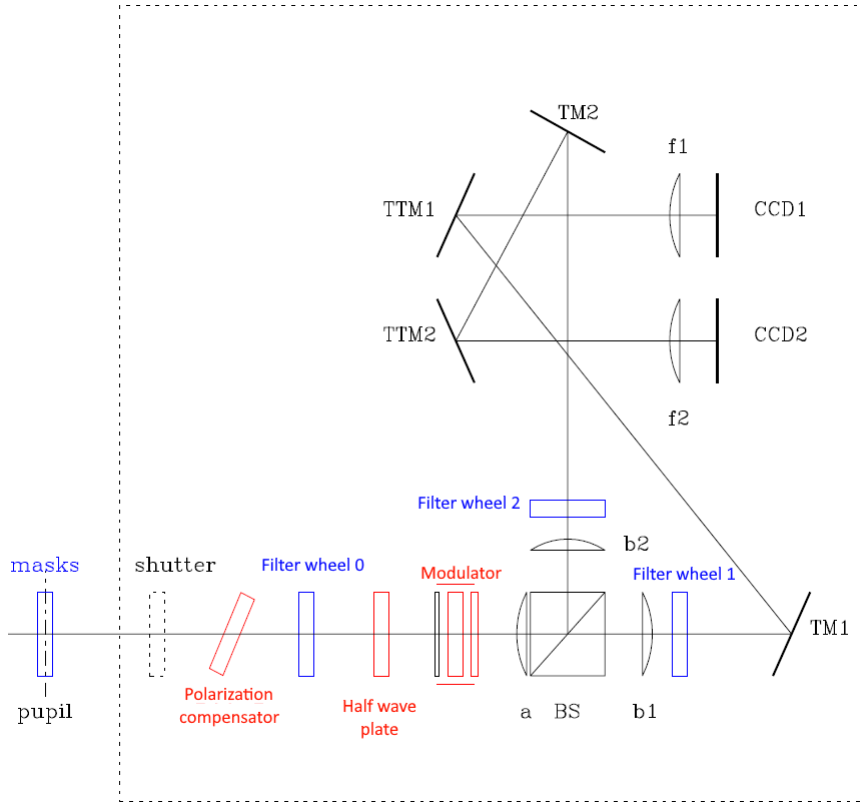


Figure 5.6: Block diagram for ZIMPOL with exchangeable components plotted in blue, while red components are only inserted for polarimetry. credit:[17]

With BS the beam splitter, TM the tip and tilted tip mirrors and a, b and f the various lenses. The polarisation compensator plate is there to reduce the retardance induced by the instrument (2 to 3 %), and more specifically by the derotator installed further up in the SPHERE instrument. The red elements can be added or removed without changing the focus of the light, allowing to switch between polarimetric imaging and regular imaging without complicated manipulations.

To eliminate atmospheric impact, a rapid modulation (1kHz) is used, this is sufficient to neglect the variations induced. This is done by a ferroelectric liquid crystal retarder (FLC) and demodulating CCD's. An FLC is a half-wave plate whose optical axis can be quickly switched by 45° when an electric current is applied. This fast switching ability comes with the price of needing a limited thermal and wavelength range (its retardance varies like $1/\lambda$). To reduce this wavelength dependency and allow a wider wavelength range, a zero order half-wave plate is used.

The polarisation is obtained by comparing intensity in two opposite linear

polarisation modes

$$p = I_{\perp} - I_{\parallel} \quad (5.5)$$

Those two modes are separated by the polarization beam splitter, a cube made out of two rectangle triangles 90° prisms of flint glass. This optical element can isolate two nearly purely polarised beams: the transmitted beam is 99.9% I_{\parallel} while the reflected beam is 97% I_{\perp} . Meaning its polarimetric efficiency is about 99.8% for the first arm and 94% on the second arm.

5.4.2 SO/PHI

The Polarimetric and Helioseismic Imager (PHI) is an instrument onboard the Solar Orbiter satellite. As its name implies, the PHI instrument is an imaging spectropolarimeter directly observing the sun. The solar orbiter was launched on february 10 2020 and is currently orbiting the sun. The instrument aims to measure external and internal solar magnetic field respectively through the impact it has on the solar light polarisation and through helioseismology.

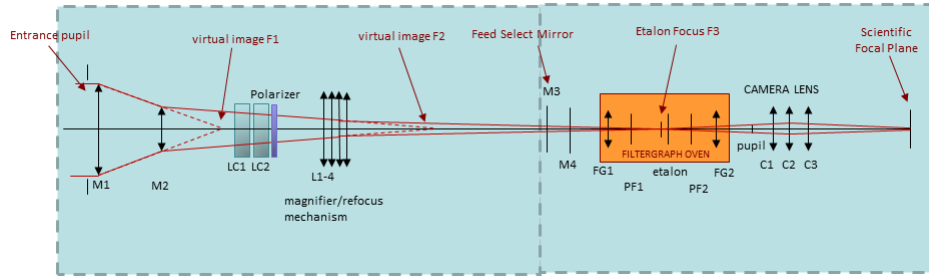


Figure 5.7: "Optics Block Diagram of the High Resolution Telescope path. M1 and M2 are the mirrors of the Ritchey-Chrétien telescope; LC1 and LC2 are the liquid crystal cells; L1, L2, L3 and L4 are the lenses of the magnifying Barlow lens system, which can be shifted to act as the refocus compensator. M3 (feed select mirror) and M4 are the folding mirrors; the Filtergraph oven includes the two lenses FG1 and FG2, the two components of the prefilter (PF1 and PF2) and the etalon; finally, the camera lenses (C1, C2 and C3) provide the image at the scientific focal plane. The beam splitter providing light to the Image Stabilisation System (ISS) is not shown." credit:[18]

The polarimeter part of the instrument uses two liquid crystal variable retarders (LCVR) and a linear polariser. The system takes four pictures in the different linear combinations of the Stokes parameters. The design isn't new, but it is the first time it is used onboard a space mission. Each polarisation detection block is made out of two antiparallel Nematic LCVRs

with their fast axis oriented at 45° with respect to each other followed by a linear polariser at 0° with respect to the fast axis of the first retarder. This last polariser serve as analyser. The test have shown an average polarimetric efficiency ϵ of (0:9917; 0:5697; 0:5666; 0:5745) for the stokes vector measurement.

The spectrometer part focuses on the detection of the Fe $0.6173 \mu\text{m}$ transition line by taking six pictures at slightly different wavelengths.

5.4.3 SPEXone

The Spectral Polarimeter for Planetary Explorations (SPEX) is an instrument of the PACE satellite whose mission is to observe the earth. Due to the recent pandemic, the launch of PACE has been delayed and will take place no sooner than 2023. SPEX's role is to measure the intensity, DoLP and AoLP of the solar light reflected on the earth surface (ocean and land) and atmosphere to detect aerosols and their concentration. These data will help in the making of more reliable climate models.

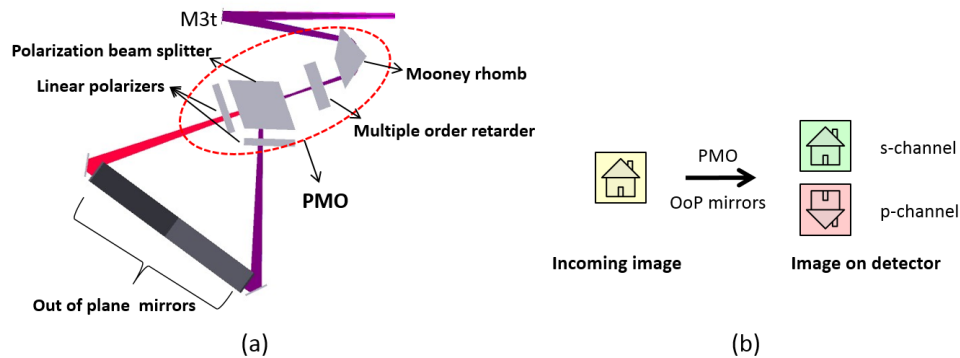


Figure 5.8: (a) Schema of SPEX's Polarisation Modulation Optics setup (b) planar symmetry of beam combining concept. credit: [19]

The polarimeter is based on spectral polarisation modulation, meaning that the radiance spectrum is modulated according to the DoLP and AoLP. The system is made out of a quarter-wave retarder, a multiple order retarder and a polarizing beam splitter assembly. This assembly converts spectral polarisation modulation into two spectrally modulated intensities by linking the amplitude of modulation with the DoLP, and the phase of the modulation with the AoLP. A Mooney rhomb (a prism that converts linear to circular polarisation) will take the role of quarter-wave retarder while the multiple order retarder will be made out of MgF_2 and quartz. The beam is then split and the two components are polarized by a set of wire-grid polarisers to achieve a polarization purity (ratio between the type

of polarisation we want and the one we don't want) higher than 1000. Their respective intensity can be expressed as [20]:

$$I_{\pm}(\lambda) = \frac{1}{2}I(\lambda)\{1 \pm P(\lambda)\cos(\frac{2\pi\delta(\lambda)}{\lambda} + 2\beta(\lambda))\} \quad (5.6)$$

The two orthogonally polarized beams are then recombined for analysis. The spectrometer design is based on an older design from the TROPOMI instrument (embarked on the Sentinel 5p satellite) using free form mirrors and a grating.

6 Modus operandi of the instrument

In this chapter, we will describe each step of the instrument and its impact on an incident polarised light. We will end by showing output signals for pure polarisation beams.

To show the effects of the setup on the incident light, let us look at an example. Here are represented the polarisation state of an incoming light at different steps of the instrument, for the following illustrations, a Stokes vector of value ($S_0 = 1500$, $S_1 = 65$, $S_2 = 37$, and $S_3 = 0$) in arbitrary intensity units, representative of a 5% degree of polarisation was used:

6.1 First wedge

Knowing the wedge fast axis angle $\alpha = 0^\circ$, and based on the previously established modulator Mueller matrix (see 5.1). We obtain the following equation for the first wedge's Mueller matrix:

$$\begin{pmatrix} 1 & 0 & 0 & 0 \\ 0 & 1 & 0 & 0 \\ 0 & 0 & \cos\Delta\phi_1 & -\sin\Delta\phi_1 \\ 0 & 0 & \sin\Delta\phi_1 & \cos\Delta\phi_1 \end{pmatrix} \quad (6.1)$$

With $\Delta\phi_1 = \frac{2\pi}{\lambda} \Delta n(\lambda)(h-y)\tan\xi$ the phase difference induced by the crossing of the wedge, $\Delta n(\lambda)$ the difference between the ordinary and extraordinary refraction indices of the element for a certain wavelength λ , and h the height of the wedge. The phase difference term lowers with the vertical position as the distance crossed by the light inside the wedge decreases.

The Stokes parameters can be represented after this first wedge as:

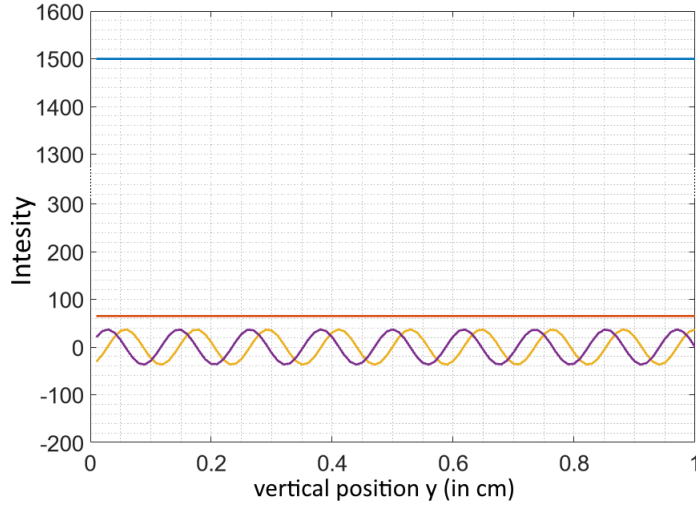


Figure 6.1: Stokes parameters values in function of the vertical positions after the first wedge. In blue S_0 , in orange S_1 , in yellow S_2 and in purple S_3 . Remark the coupling between S_2 and S_3 induced by the wedge.

In this setup, the role of a wedge is to couple two Stokes parameters, in our case the first wedge couples the last two Stokes parameters (the diagonal linear polarisation and the circular polarisation degree). We see that neither the intensity nor the other Stokes parameter (here U , the first linear polarisation term) are impacted, and that a sinusoidal pattern has appeared on the diagonal and the circular polarisation terms. This is due to the nature of the modulator: the modulator act as a retarder, rotating the polarisation state between S_2 and S_3 , as the angle of rotation varies along the vertical, we cover the whole circle several times.

This coupling can be clearly seen in the matrix associated with the element, and as the variation of $\Delta\phi$ along y is sinusoidal, so is the one of the coupled output elements.

6.2 Second wedge

The second wedge does not influence the polarisation state of the crossing light, and is just there to prevent medium changes effects while making the system sturdier. To manage this, we fix its fast axis parallel to the z axis (the progression direction of the light), in other words, we set its fast axis angle $\alpha = \frac{\pi}{2}$.

6.3 Third wedge

The transformation matrix associated with the third wedge is expressed as:

$$\begin{pmatrix} 1 & 0 & 0 & 0 \\ 0 & \cos\Delta\phi_3 & 0 & \sin\Delta\phi_3 \\ 0 & 0 & 1 & 0 \\ 0 & -\sin\Delta\phi_3 & 0 & \cos\Delta\phi_3 \end{pmatrix} \quad (6.2)$$

With $\Delta\phi_3 = \frac{2\pi}{\lambda} \Delta n(\lambda)(h-y)\tan\Psi$ the phase difference induced by the wedge, similarly to the first one. Just like we did with the first wedge, we can represent the Stokes parameter values after the wedge in function of their vertical position y .

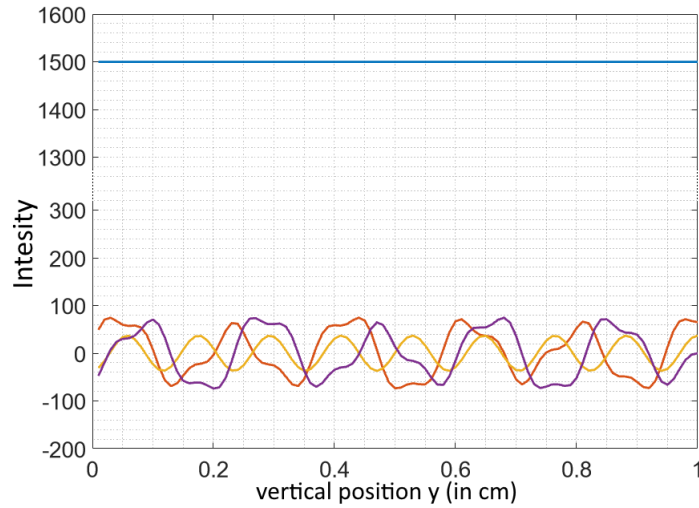


Figure 6.2: Stokes parameters values in function of the vertical positions after the third wedge. In blue S_0 , in orange S_1 , in yellow S_2 and in purple S_3 . Remark now the coupling between S_1 and S_3 induced by the wedge.

The role of the third wedge is to couple the circular polarisation term with the remaining linear polarisation term. This time it is the intensity and the second linear polarisation term that remains unchanged. We can see the apparition of a more complex pattern, resulting from the superposition of two sinusoidal variations.

6.4 Analyser

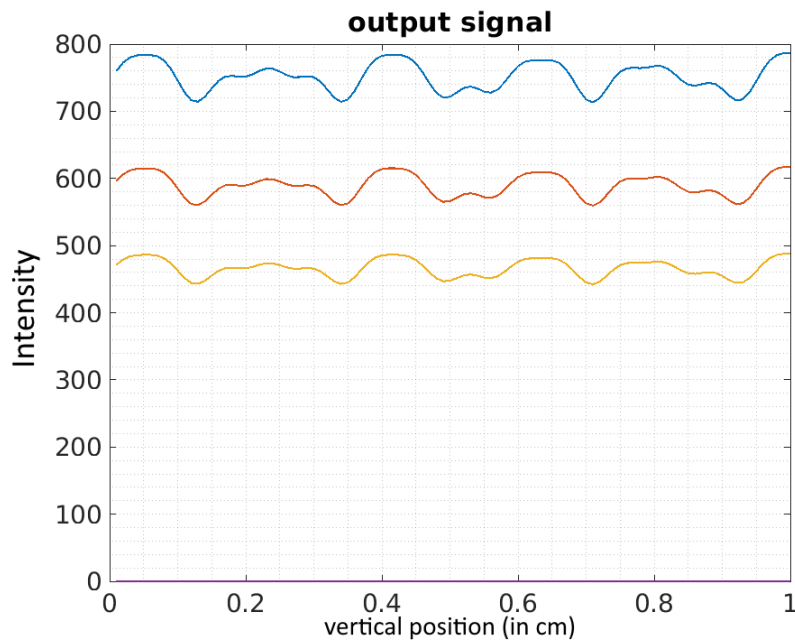


Figure 6.3: Stokes parameters values in function of the vertical positions after the analyser. In blue S_0 , in orange S_1 , in yellow S_2 and in purple S_3 . We see similar pattern for all except S_3 , blocked by the analyser.

Like said in the previous chapter, the role of the analyser is to couple all the linear polarisation parameters with the intensity. Here We also represented the Q and U polarisation state, even if we cannot measure them, to show that they present a similar exiting pattern as the intensity. The transformation matrix associated with the analyser has already been described in the previous section.

6.5 Values for typical polarisation vectors

In this section, we will show the output signal of the instrument for various typical polarisation. With each case is written the associated specific stokes vector, this vector is unique, as what has been proved in the 2020 Vasilescu et al paper ([15]).

Non polarised Beam Let us study the image of the Stokes vector $S=(1,0,0,0)$

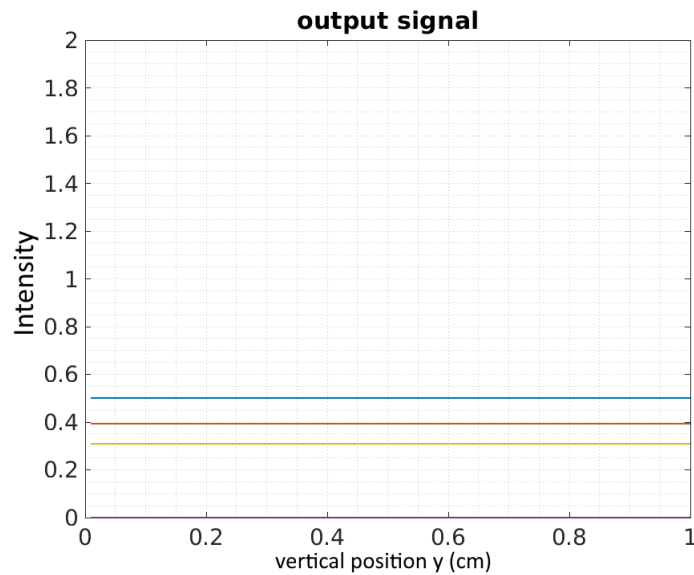


Figure 6.4: Output Stokes parameters of a non polarised beam in function of the pixel's vertical position. In blue S_0 , in orange S_1 , in yellow S_2 and in purple S_3 . Remark the absence of pattern due to the absence of polarisation.

Intuitively, we could have expected this result: The instrument is made to create a variation based on the polarised part of the beam, and since there is no polarisation, the output signal is not modulated.

Parallel (0_x) Then the image of the Stokes vector $S=(1,1,0,0)$

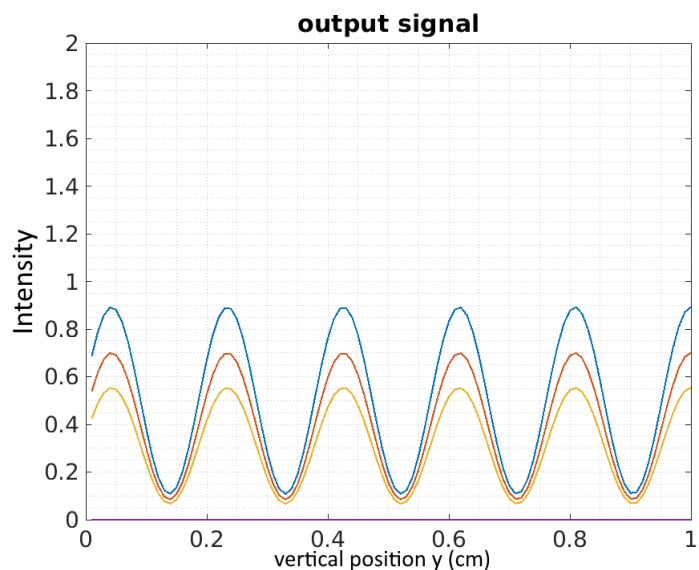


Figure 6.5: Output Stokes parameters of a horizontally polarised beam in function of the pixel's vertical position. In blue S_0 , in orange S_1 , in yellow S_2 and in purple S_3 . Sinusoidal pattern due to only one coupling of parameters

Perpendicular (0_y) The image of the Stokes vector $S=(1,-1,0,0)$

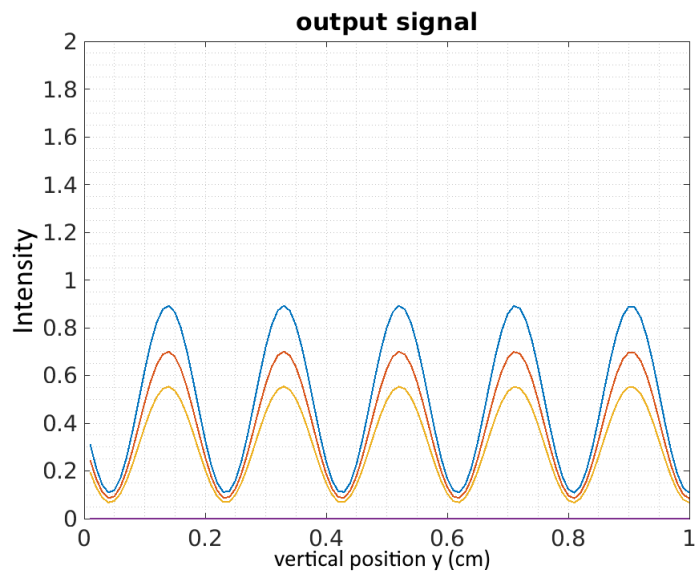


Figure 6.6: Output Stokes parameters of a vertically polarised beam in function of the pixel's vertical position. In blue S_0 , in orange S_1 , in yellow S_2 and in purple S_3 . Sinusoidal pattern due to only one coupling of parameters

For both parallel and perpendicular polarisation, we see a sinusoidal pattern appear. This is due to the fact that Q only feels the influence of the second wedge, that link Q and V, and not the first wedge. So the system behaves like if there was only one wedge.

Diagonal (+45°) The purely diagonal Stokes vector $S=(1,0,1,0)$

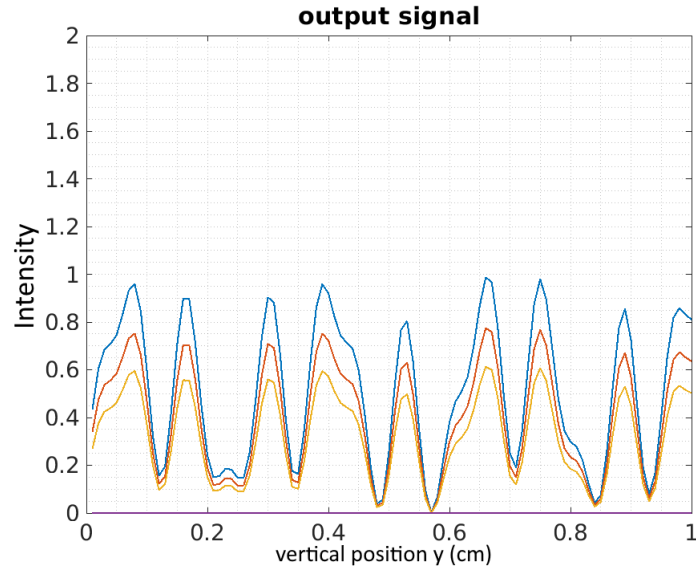


Figure 6.7: Output Stokes parameters of a diagonally polarised beam in function of the pixel's vertical position. In blue S_0 , in orange S_1 , in yellow S_2 and in purple S_3 .

Anti diagonal (-45°) The antidiagonal Stokes vector $S=(1,0,-1,0)$

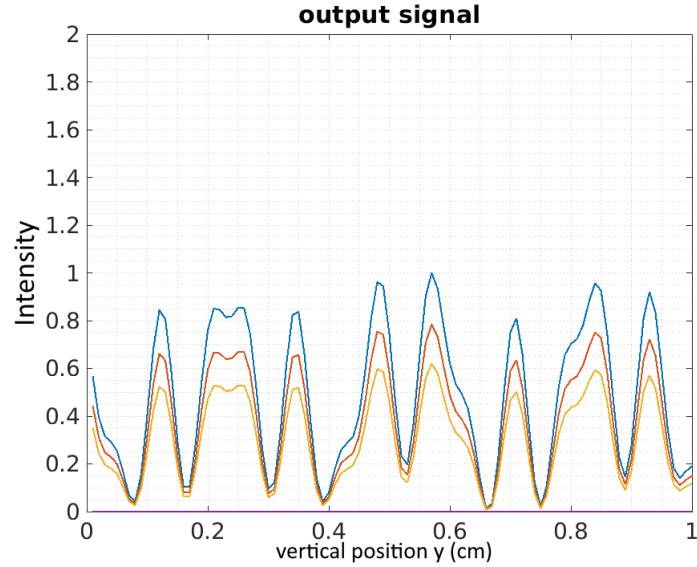


Figure 6.8: Output Stokes parameters of a anti diagonally polarised beam in function of the pixel's vertical position. In blue S_0 , in orange S_1 , in yellow S_2 and in purple S_3 .

For both diagonal and anti diagonal polarisation, we see a complex pattern, superposition of two sinusoids, appear. Even though U only feels the influence of the first wedge, the coupling with V has propagated this perturbation to all the polarisation parameters after the second wedge. At the exit of the first wedge, the pattern presented by the light is similar to the one shown previously, except that the oscillations are on the diagonal and circular polarisation terms.

Right circular (RCP) Stokes vector $S=(1,0,0,1)$

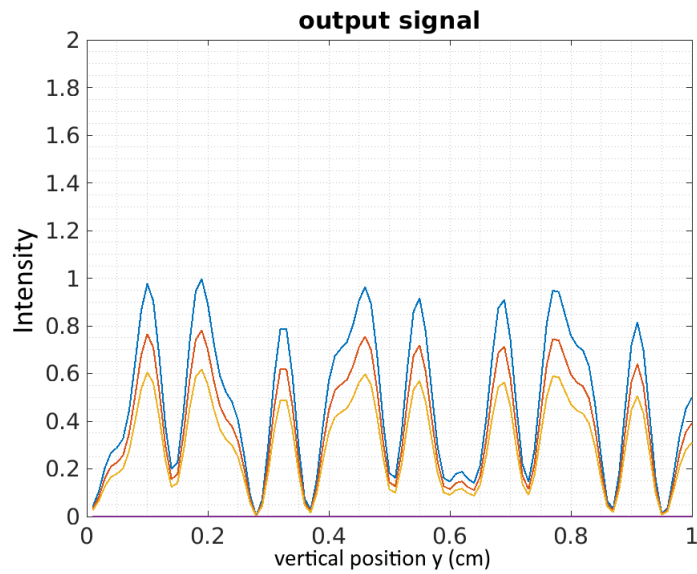


Figure 6.9: Output Stokes parameters of a right circularly polarised beam in function of the pixel's vertical position. In blue S_0 , in orange S_1 , in yellow S_2 and in purple S_3 .

Left circular (LCP) Stokes vector $S=(1,0,0,-1)$

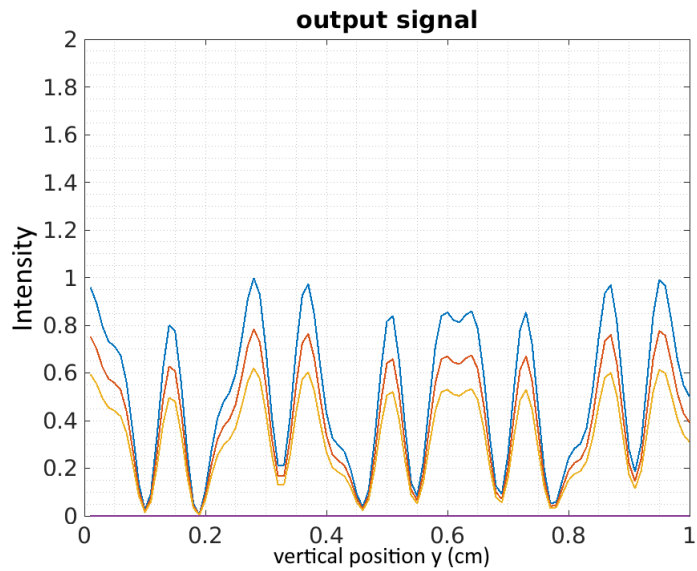


Figure 6.10: Output Stokes parameters of a left circularly polarised beam in function of the pixel's vertical position. In blue S_0 , in orange S_1 , in yellow S_2 and in purple S_3 .

For both circular polarisation, we see a complex pattern, similar to the one observed with the previous step, appear. The two signals are similar since both the diagonal polarisation and the circular polarisation are modulated twice. The output beam does not show circular polarisation (in purple) because it is blocked by the analyser (see the analyser Mueller matrix).

7 Simulations

This chapter is the core of the work, this is where we will try and test the robustness of the output signal to perturbations of the input signal. The goal is to estimate which precision is reached when reconstructing the initial parameters after the instrument. At each step will be shown graphs of the parameters' values before the instrument (left graphs), and when imprecision appears, the highest and lowest values obtained at the output of the instrument (right graphs). These values will help us to see the maximum deviation caused by the perturbation we studied.

The first part of the work consisted of the simulation of the instrument, to see the output signal associated with various polarised inputs. For that, we wrote a mathematical model simulating the impact of the instrument on the stokes parameters.

7.1 Algorithm

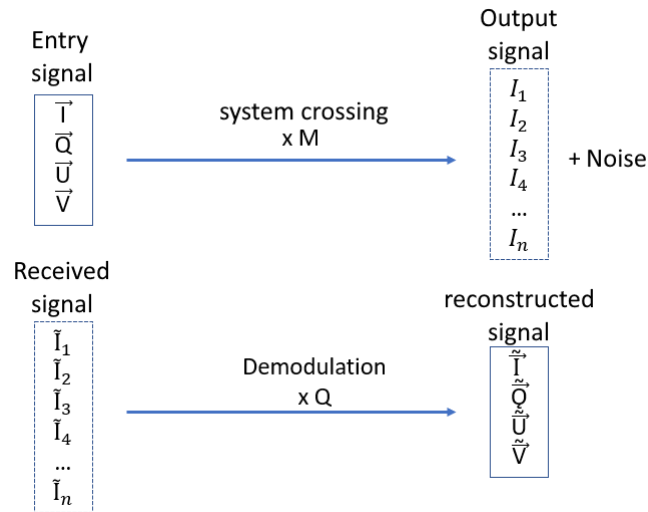


Figure 7.1: Schematic view of the used algorithm

The program we used works in two steps: first, it takes a series of Stokes vector (one for every vertical position) and multiplies each of them with the Mueller matrix of the instrument. By taking the S_0 term of the produced stokes vectors, it generates an output intensity vector the same length as

the number of pixel of the instrument.

It then takes this output intensity vector and transforms it back into Stokes vectors by multiplying each elements by the pseudo inverse of the instrument's Mueller matrix.

Another possible technique uses a fit of the output intensity vector using the reference output signals obtained in the previous section (section 6.5).

Starting from the last chapter's equations, we get that the output matrix of the system is given by:

$$S_o(\theta, y, \lambda) = \frac{1}{2} \begin{pmatrix} I + Qcc_3 + U(sc_1 + cs_1s_3) + V(cc_1s_3 - ss_1) \\ Ic + Qc^2c_3 + Uc(sc_1 + cs_1s_3) + Vc(cc_1s_3 - ss_1) \\ Is + Qscc_3 + Us(sc_1 + cs_1s_3) + Vs(cc_1s_3 - ss_1) \\ 0 \end{pmatrix} \quad (7.1)$$

with once again $c_1 = \cos\Delta\phi_1$, $s_1 = \sin\Delta\phi_1$, $c_3 = \cos\Delta\phi_3$ and $s_3 = \sin\Delta\phi_3$. The only thing that interest us is the \tilde{S}_0 term (the intensity), since it is the only parameter measurable by the detector.

The measured output signal is thus given by:

$$\tilde{I}(\theta, y, \lambda) = \frac{1}{2}(I + Qcc_3 + U(sc_1 + cs_1s_3) + V(cc_1s_3 - ss_1)) \quad (7.2)$$

That we can then reproduce for every pixel centre position y .

With this notation, the dependancy of \tilde{I} to y is not obvious, as it is hidden in the c_1, s_1, c_3 and s_3 terms. One can pose another notation, developed in [15], such that

$$d(\theta, y, \lambda) = c * c_3 \quad (7.3)$$

$$e(\theta, y, \lambda) = s * c_1 + c * s_1 * s_3 \quad (7.4)$$

$$f(\theta, y, \lambda) = c * c_1 * s_3 - s * s_1 \quad (7.5)$$

For a detector made out of n pixels, we end up with a n -length vector expressing the output intensity in function of the vertical position.

$$\tilde{I}(\theta, y_1, \lambda) = \frac{1}{2}(I + Q * d(\theta, y_1, \lambda) + U * e(\theta, y_1, \lambda) + V * f(\theta, y_1, \lambda)) \quad (7.6)$$

$$\tilde{I}(\theta, y_2, \lambda) = \frac{1}{2}(I + Q * d(\theta, y_2, \lambda) + U * e(\theta, y_2, \lambda) + V * f(\theta, y_2, \lambda)) \quad (7.7)$$

$$\dots \quad (7.8)$$

$$\tilde{I}(\theta, y_n, \lambda) = \frac{1}{2}(I + Q * d(\theta, y_n, \lambda) + U * e(\theta, y_n, \lambda) + V * f(\theta, y_n, \lambda)) \quad (7.9)$$

7.1.1 Inverse Matrix technique

Now that we have the instrument's output signal, we can try to reconstruct the initial Stokes parameters by inverting the relation.

Since our Mueller matrix is not symmetric, we cannot easily obtain its inverse. We thus have to use a pseudo inverse matrix D (for demodulation) given by the equation:

$$D = (O^T O)^{-1} O^T \quad (7.10)$$

so that $D.O = Id$. This matrix is then used to inverse the effect of the instrument and reconstruct the initial Stokes parameters. We then obtain:

$$\tilde{S}_{in}(i) = \sum_{j=1}^N D_{ij} \tilde{I}(j) \quad i = 1, 2, 3, 4 \quad (7.11)$$

The unicity of this solution has been previously proven [15].

This is the technique we will be using for our simulations.

7.1.2 Signal fitting

Another way to find the initial parameters starting from the output signal is by fitting it. This allows the exploitation of the signal even if we do not know the properties of the instrument or cannot obtain the matrix D . However this situation shouldn't appear as the instrument properties can easily be obtained during the calibration phase or by observing a known source during operation.

This technique can lead to imprecision at lower pixel count since the fit remains only an approximation of the real values.

7.2 Instrument precision

Now that we know how does the instrument works, we can establish a first theoretical estimation of its precision.

We know the expression of the output signal (equation 7.2), and we know the resolution is fixed by vertical (y) elements (the size of the pixels). Using the dephasage expressions, we see that the variation of $\Delta\phi_3$ can be expressed as $\frac{2\pi}{\lambda} \Delta n(\lambda)(-\Delta y) \tan\Psi$, and similarly for $\Delta\phi_1$ as $\frac{2\pi}{\lambda} \Delta n(\lambda)(-\Delta y) \tan\xi$.

We introduce the values used in Vasilescu et al paper ([15]), that are also used in the following simulations. We thus have $\lambda = 6.3 * 10^{-7}m$, $\Delta n(\lambda) = 0.0118$ for the material used, $\Psi = 1.6^\circ$ the angle of the third wedge, $\xi = 2.6$ the angle of the first wedge, and $\Delta y = 10^{-5}m$ the length of one pixel.

The values are thus $\Delta\phi_3 = \pm 0.0164^\circ$ and $\Delta\phi_1 = \pm 0.027^\circ$. These values translate (for the worst ϕ possibles, even if this case do not present itself) as a maximum imprecision of $\Delta I = \pm \frac{1}{2}(S_1 * (3.88 * 10^{-5}) + S_2 * (1.96 * 10^{-4} + 1.17 * 10^{-4}))$.

$10^{-8}) + S_3 * (1.17 * 10^{-8} - 1.96 * 10^{-4})$, or around $\Delta I = \pm 2 * 10^{-4} (\frac{S_1}{10} + S_2 + S_3)$. This value is smaller than the noise that can appear on the detector.

7.3 Simple signal

The first signals we submitted to the program did not vary over time, to see if everything worked properly. This simplified problem allows us to see if we could reconstruct correct values at the end of the system, and quantify the eventual bias that could arise.

7.3.1 Without noise

For the first step, we generated various signals with uniformly fixed values of polarisation degree (the percentage of the light that is polarised) devoid of noise that were submitted to the program. For simplicity, we considered a uniform intensity of 1500 photon count on each pixel of the detector, and a detector 1.3 cm long made out of 1300 pixels. We also consider purely linear polarisations. The addition of circular polarisation would only complexify the output signal without significantly impacting the precision of measurements.

This step allows us to see the typical output signal of our system before perturbation.

At each step we also expressed the visibility value, as a reminder, the visibility is a dimensionless number expressing the contrast of the signal.

Mid range estimation: (5%) This will be the reference degree of polarisation used during the next steps. The value of 5% polarisation is based on an average DoLP measurement during the previous auroras observations.

The visibility is here 0.0328. This value will serve as reference.

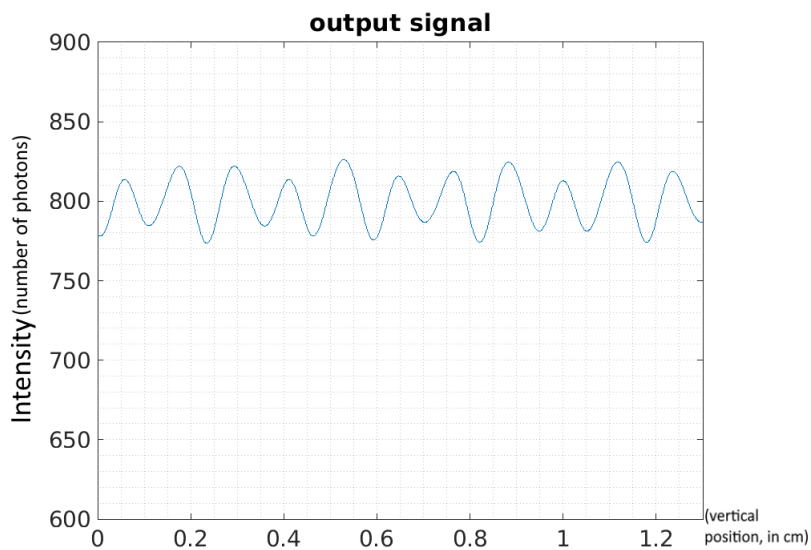


Figure 7.2: Output intensity associated with a 5% linear polarisation degree in function of its vertical position y on the detector

Highest estimation (10%) With 10% polarisation, we see that the output graph shows bigger amplitude oscillations. Like for the 5%, the value of 10% is an upper estimations based on the previous observations campaigns.

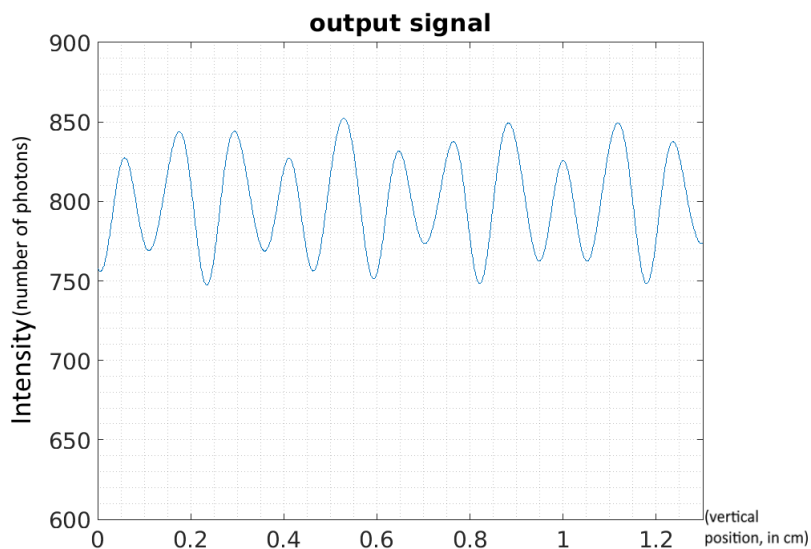


Figure 7.3: Output intensity associated with a 10% linear polarisation degree in function of its vertical position y on the detector

The visibility is here 0.0656. We see that the visibility augments when the percentage of light that is polarised increases.

Low polarisation estimation (1%) As we can see, the 1% polarisation shows less intense signal variations.

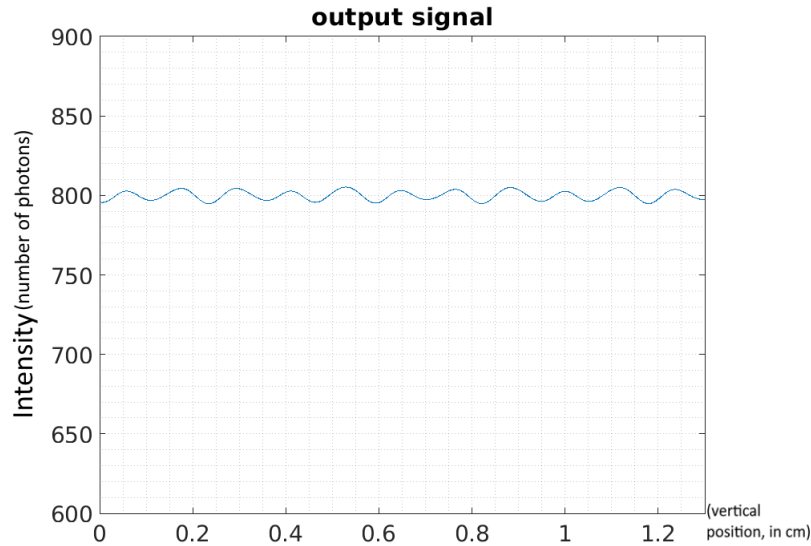


Figure 7.4: Output intensity associated with a 1% linear polarisation degree in function of its vertical position y on the detector

And the visibility is smaller, with a value of 0.0066.

What we can deduce from these results is that the DoLP value only affects the oscillation amplitude of the output signal (and thus the visibility), but not the output signal's pattern.

These results also show that this amplitude change is directly proportional to the DoLP. The oscillation pattern can only be changed by varying the ratio of the Stokes parameters, as seen in the previous chapter.

We can also see that even before perturbation the visibility value isn't that large due to the low polarisation degree we work with.

Talking about the precision for this section wouldn't make sense, as we consider having a perfect knowledge of the parameters at every steps.

signal discretisation

Since we use the number of photons received as a measure of the intensity parameter, we have to discretise the output intensity values to stay

coherent, as there is no such thing as partial photons. To evaluate the impact of this manipulation, we studied a light 10 times fainter than before, as discretisation should only impacts very low intensity signals, which would be the most sensitive to shot noise anyway.

On this graph, we represented the highest (red) and lowest (blue) reconstructed values of the parameters obtained during simulation. On the left are the parameter values before the instrument, and on the right the reconstructed values and their associated imprecision. The first simulation was without noise:

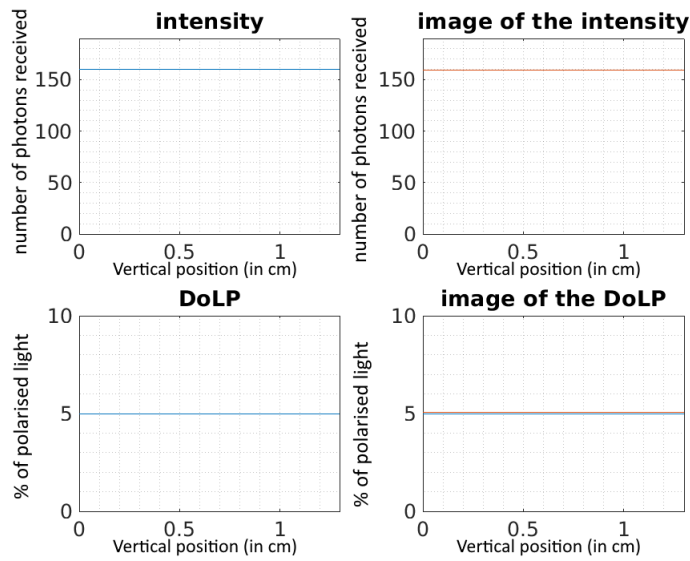


Figure 7.5: Variation of the main parameters (I and DoLP) in function of their vertical position before and after the instrument in case of low light levels. The intensity is expressed in number of photon and the vertical position in cm.

We see that despite the discretisation of the output signal the system is quite robust: The imprecision on the intensity is nearly nonexistent, as is the one on the degree of polarisation (less than 2% of the polarisation degree value). The visibility is here 0.0314 without noise. This indicates that the discretisation of the output signal shouldn't induce too many perturbations at higher light levels.

A second simulation at low light level was realised to incorporate noise, and is thus located in the relevant noise section 7.3.2 later in this paper.

7.3.2 Impact of perturbations on the expected precision

We then studied the impact of various type of input parameters perturbation on the output signal, and the imprecision induced on the reconstructed stokes parameters. To be able to compare the different results, we took a fixed input Stokes vector:

$$S = \begin{pmatrix} 1500 \\ 65 \\ 38 \\ 0 \end{pmatrix} \quad (7.12)$$

Corresponding to an arbitrarily fixed 5% linearly polarised incoming beam.

Input intensity perturbation

The first case we studied was a perturbation on the input intensity parameter. We studied two cases: a random low amplitude perturbation, called "noise like variation", and a progressive continuous decrease of the parameter, called "continuous variation".

Noise like variation

We first apply a random low amplitude (2% of the intensity) perturbation. This could be seen as a perturbation of the initial intensity by the atmosphere.

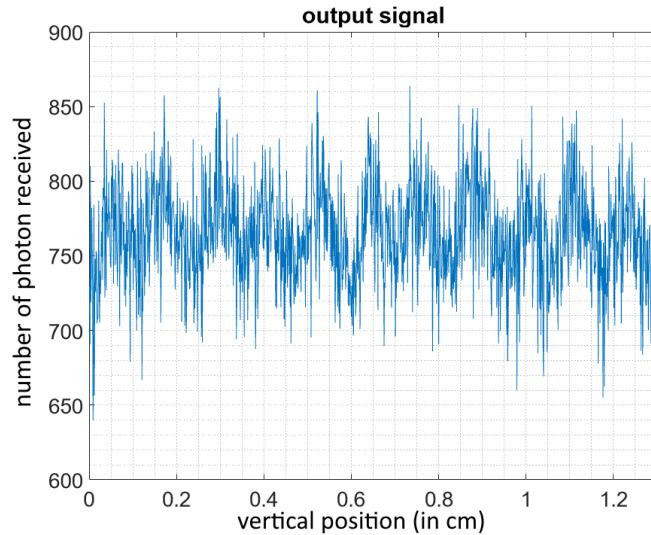


Figure 7.6: Output intensity signal (number of photons)in function of the pixel vertical position y

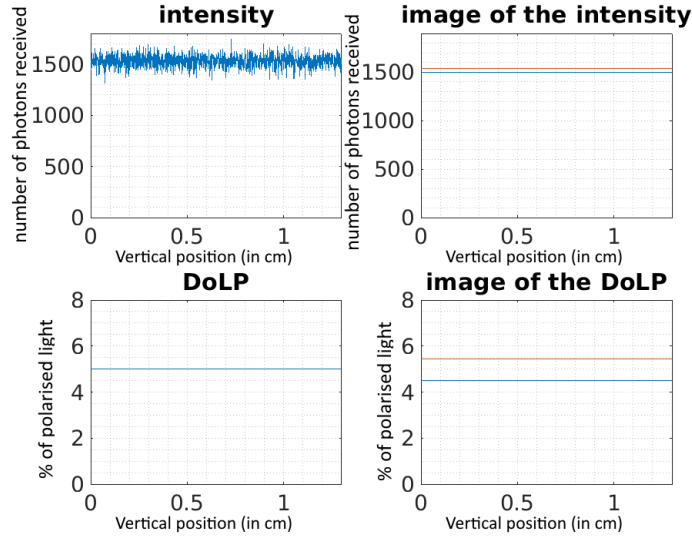


Figure 7.7: Impact of an intensity noise on the main parameters' precision. Highest (red) and lowest (blue) output values are represented on the output graphs (on the right).

Once again the highest (red) and lowest (blue) output values are represented on the output graphs (on the right). We see that the impact of the noise on the visibility value (here 0.1446) is more important than its impact on the reconstructed Stokes parameters' precision.

The perturbations on the input intensity directly propagate to the output signal (the output intensity) and to the other parameters values, S_1 and S_2 , as they are proportional to the intensity. This affects the system ability to give correct output values, as it changes the shape of the signal. The resulting imprecision is directly related to the amplitude of these intensity variations, with here a nearly ± 0.5 imprecision on the DoLP (10% of its value), and a very small imprecision on the intensity (3% of its value). However, the reconstructed values in themselves won't show any variations, as they are averaged by the system.

Continuous variation

We then study a continuous variation, here a continuous decrease, to represent the growing distance from the source to the detector over the instrument field of view.

After compensation for the varying intensity, we found a visibility of 0.0465. We see that the impact of this variation is way less important than

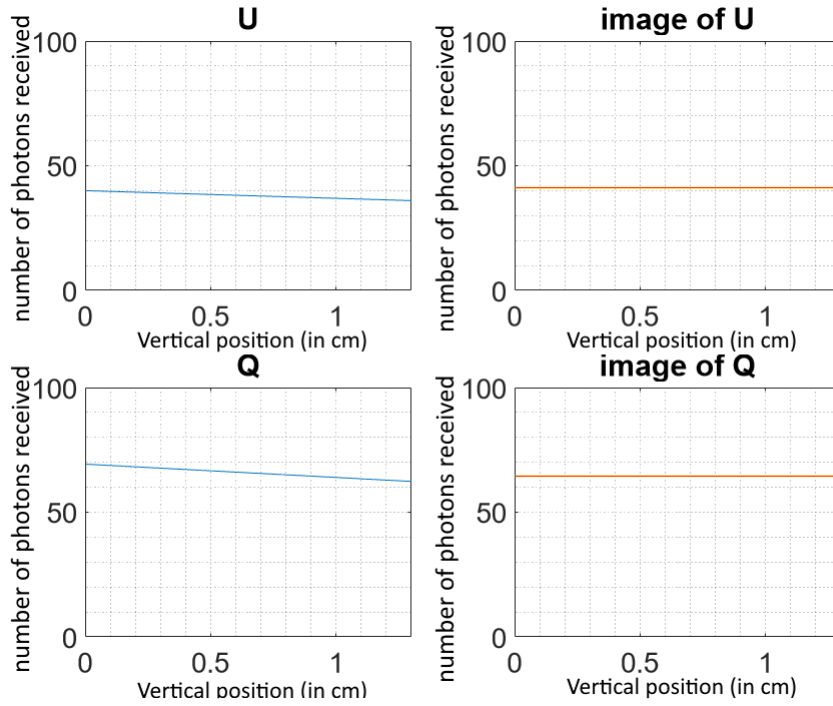


Figure 7.8: Impact of continuous intensity variation on the linear polarisation parameters's output values

the one of the random variation.

As we can see, the impact on U and the intensity, and on the Q output isn't the same, the U parameter undergoing an averaging the same order as the intensity, while the Q parameter is lowered. This is linked to the angles ξ , ψ and θ we used for our simulation, with different values giving different ratios of variation for U and Q. Other than that averaging, we see no imprecision on the reconstructed stokes parameters values induced by this variation.

Of course in reality the intensity variation isn't as extreme as described in the previous simulation due to the small field of view covered.

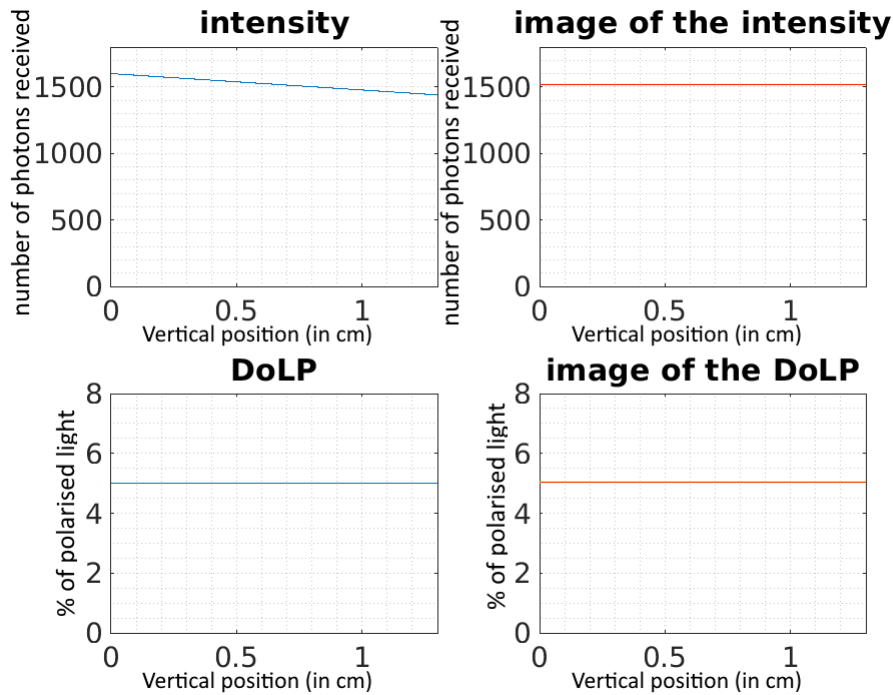


Figure 7.9: Impact of continuous intensity variation on main parameters's output values

Polarisation perturbation

Then we applied the same random low amplitude perturbation to the degree of polarisation value, to simulate the impact of spatially varying polarisation and pollution reaching the detector.

The visibility is here 0.0361. This low value confirms the very low impact of the polarisation variation on the precision of the system.

Just like for the intensity noise, all the small variations are averaged by the system.

To be able to detect those spatial variations (in intensity or in polarisation) would require the subdivision of the output signal in different blocs that overlap each other, followed by the analysis of all these individual blocs by the system. This would lead to the increase of steps needed to analyse every part of the signal, as you would need to analyse each bloc every time which would multiply the amount of data that has to be treated and stored and a longer integration time. This approach will be investigated in the next chapter.

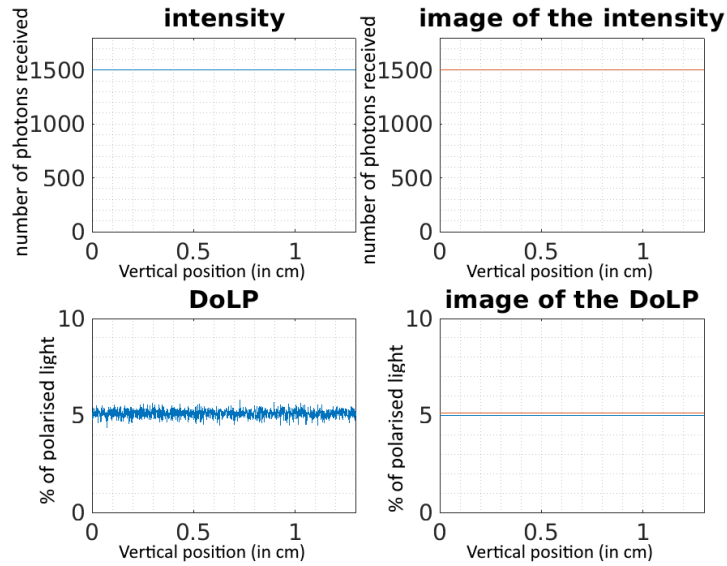


Figure 7.10: Intensity and polarisation before and after the instrument in case of noise on the polarisation degree parameter

Continuous variation

Continuously varying the DoLP would only show an averaging of the output parameters and not bring any new pieces of information.

The next step would have been to study the same sort of perturbations on the Q and U parameters, however to simply study the impact of Q or U variation would just show similar results as the one obtained during polarisation degree perturbation since they are intrinsically linked. So we have to change the ratio of U and Q instead. This variation is not that interesting to show, as it only modifies the shape of the output signal, but do not impact the precision of the other output parameters reconstruction. We only see averaged values of U and Q, as was expected from the previous observations.

We also studied the impact of spikes in the measurements. As we have seen in the previous paragraphs all output values are averaged, so the inclusion of spikes in the measurements only translates as an increase of the output parameters value. This lead to imprecision in the parameters reconstructions.

Signal noise

Finally, we implemented the noise, described earlier in section 4.2, affecting the output signal before deconvolution and studied the imprecision

induced on the rebuilt parameters. This can be seen as errors on the detector itself, inherent to every sensor.

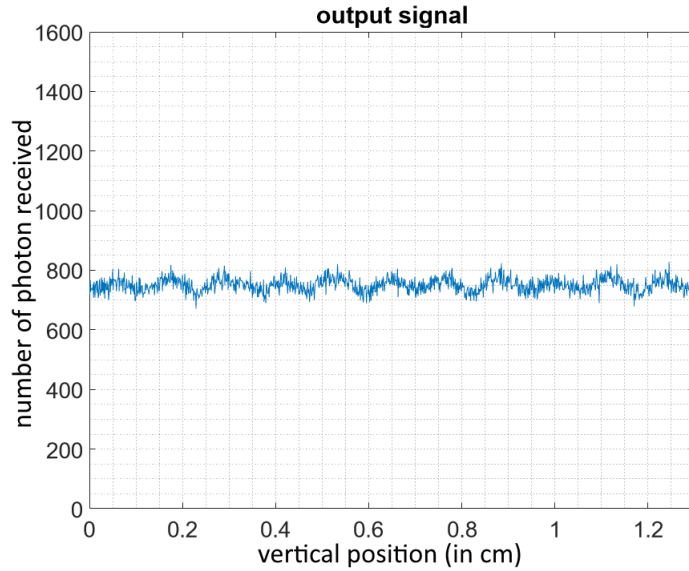


Figure 7.11: Typical output signal with the added noise perturbations

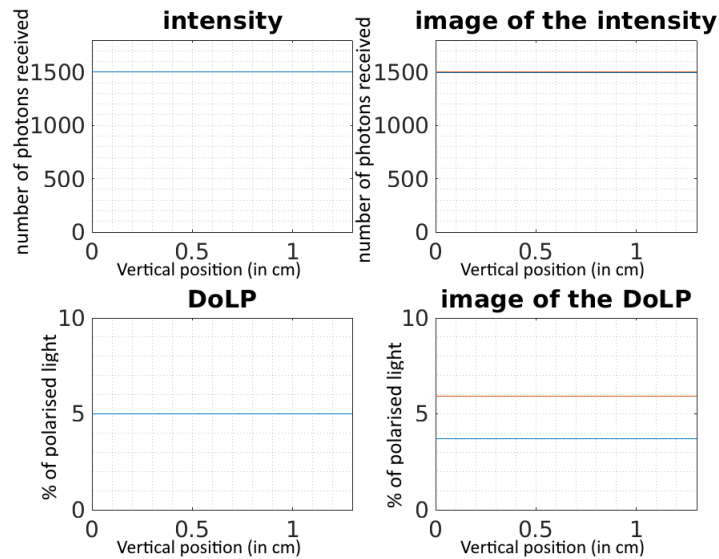


Figure 7.12: Modification of the I (up) and DoLP (down) parameters before (left) and after (right) the instrument in case of signal noise. Once again the highest (red) and lowest (blue) values are represented.

The visibility is here 0.0337

As we can see there is an impact on the polarisation term, and on the precision of our instrument, the order of 20% of the DoLP value. The presence of noise on the output signal is the main source of imprecision of our system. As we are talking about regular noise, this imprecision can be reduced by observing higher intensity signal.

Low intensity Let us take the low intensity case once more, but this time with noise. We see that we get a very different result:

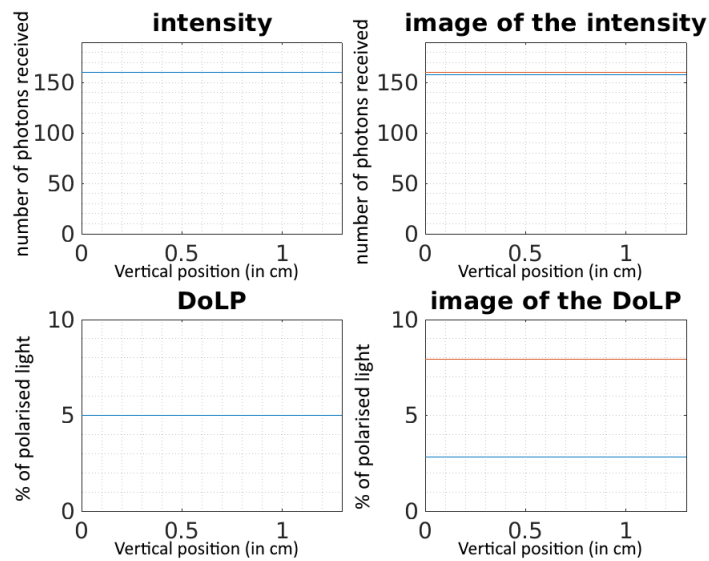


Figure 7.13: Variation of the main parameters (I and DoLP) in function of their vertical position before and after the instrument in case of noisy low light levels. The intensity is expressed in number of photons and the vertical position in cm.

We see that the imprecision on the degree of polarisation becomes quite important (± 3 , or 60% of the DoLP), while the imprecision on the intensity value isn't really impacted. We also have a value of the visibility that gets up to 0.356. These high values of the visibility and DoLP imprecision are due to the low signal and the impact of the noise, which creates variations the same order as the signal. This means that the precision of our instrument suffer greatly when we try to observe signals that are too faint.

7.3.3 Main source of imprecision

At the end of this section, we see that the main source of imprecision that will impact our system is the one affecting the signal received by the detector. This imprecision (the order of 20 % of the DoLP value for the Stokes vector we used) is inversely proportional to the intensity of said signal.

7.4 "Realistic" signal

The second part of the work was to expose our model to a more realistic time varying signal.

For this, we generated a signal pseudo randomly varying between the observed maximal and minimal values of auroral light polarisation (1 to 5% [10]) before submitting it to the program. To achieve this, we set each step as a uniform signals (with noise) on which we applied a pseudo random variation (limited in amplitude and applied uniformly on the whole signal) to go from step to step.

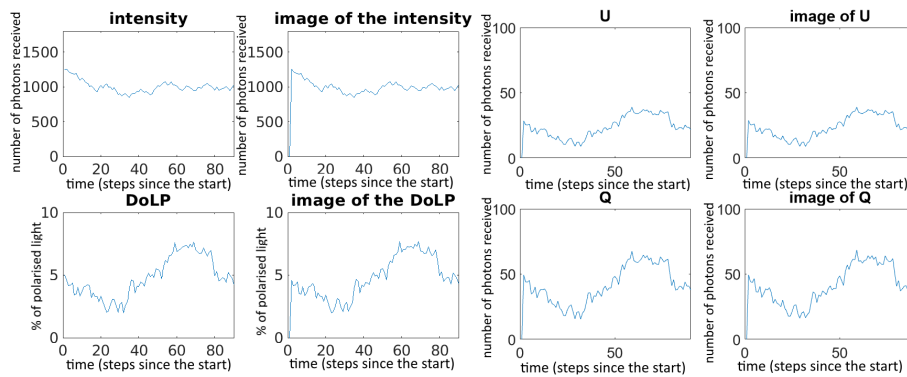


Figure 7.14: Intensity (upper left graphs), DoLP (lower left graphs), U (upper right graphs) and Q (lower right graphs) values before and after the instrument in function of the time. Each step represent an observation period

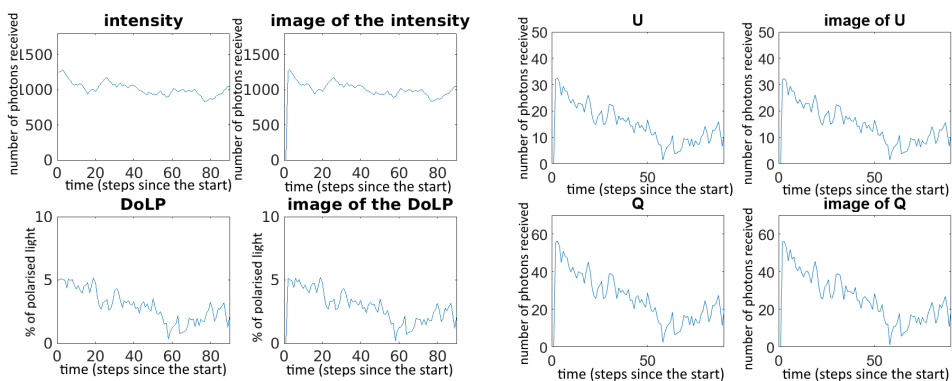


Figure 7.15: Same initial parameters, but for another run

We can see that the input and output signal shapes are similar, which is a good news. This step allows us to evaluate the capacity of the system to transmit a general time variation pattern inscribed on the incoming light to the outgoing reconstructed parameters. More than the exact value of the DoLP, the general shape of its evolution can help us link it with the observed phenomena happening during the observed periods.

8 Possible instrument optimisation

In this short chapter we explore ways of improving the reconstruction precision, and to include a bit of spatial resolution.

As of the way to optimise this instrumental approach to the observation of auroras, the main objective would be to find a way to do the longest exposure possible on this short varying phenomenon, or to increase the amount of light entering the detector. Auroras are a faint phenomenon, and this low signal is the main problem when we will want to limit the noise impact.

8.1 Change in the pixel amount

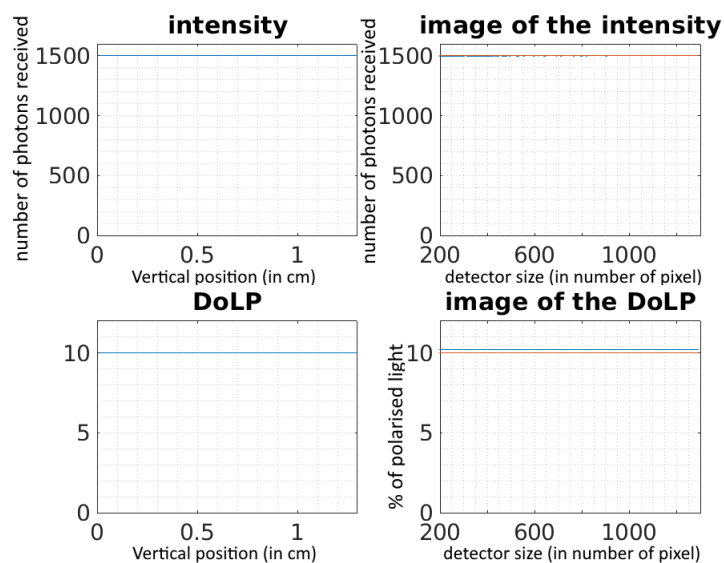


Figure 8.1: Intensity (upper graphs) and DoLP (lower graphs) values before and after the instrument when we vary the number of pixels composing the detector (the number of pixels is given on the horizontal axis).

The way of solving this problem that we investigate was to use a lower number of pixels. To investigate the impact of this manipulation we varied the number of pixels present at the end of the instrument, to see the lowest amount needed to correctly be able to find the initial Stokes parameters back after the crossing of the instrument. By lowering the number of pixels, we decrease the SNR by increasing the value of the intensity, but decrease

the precision of measurement. This is similar to the "binning" technique: we combine pixels values before analysis so the detector works as if we were using bigger pixels. This allows more photons to be collected without physically changing the setup.

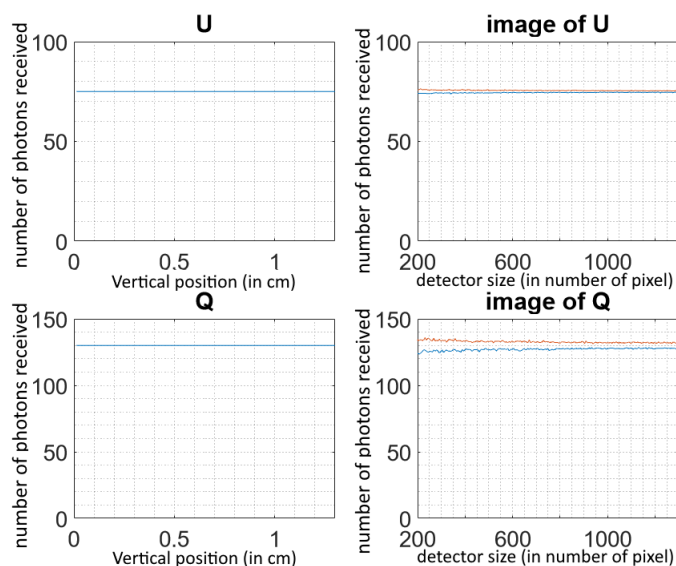


Figure 8.2: U (upper graphs) and Q (lower graphs) values before and after the instrument when we vary the number of pixels composing the detector (the number of pixels is given on the horizontal axis)

We can see that as we increase the number of pixels from 200 to 1300 by regular steps, the sensitivity to noise decreases but the precision remains approximately the same. This is not the case at a very low number of pixels as the system has more difficulties reconstructing the initial set of parameters with fewer points.

8.2 Increasing spatial precision by splitting the output signal

The second thing we wanted to investigate was the effects of subdividing the output signal into blocks. This subdivision is done on the output signal, allowing the analysis of each block like a detector signal of its own. This allows us to add a spatial dimension to our results.

The first thing we expected to see was a small decrease in precision due to the lower amount of pixels, as shown in the previous section. Combined with the limited size of the detector, this should imposes an upper limit in

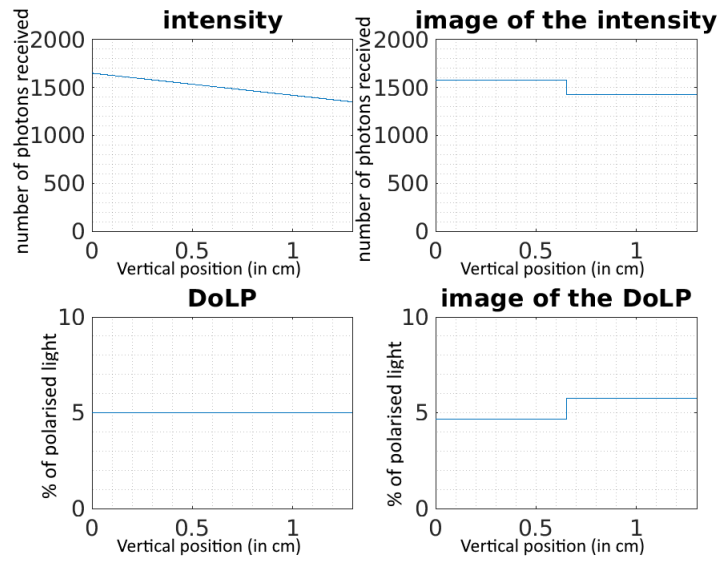


Figure 8.3: I (upper graphs) and DoLP (lower graphs) values before and after the instrument when we subdivide the detector output signal in two blocks before analysis

the number of blocks possible if we want to be able to reliably use the data. However that's not what we see. And when we look at the U and Q values, we observe the same phenomenon.

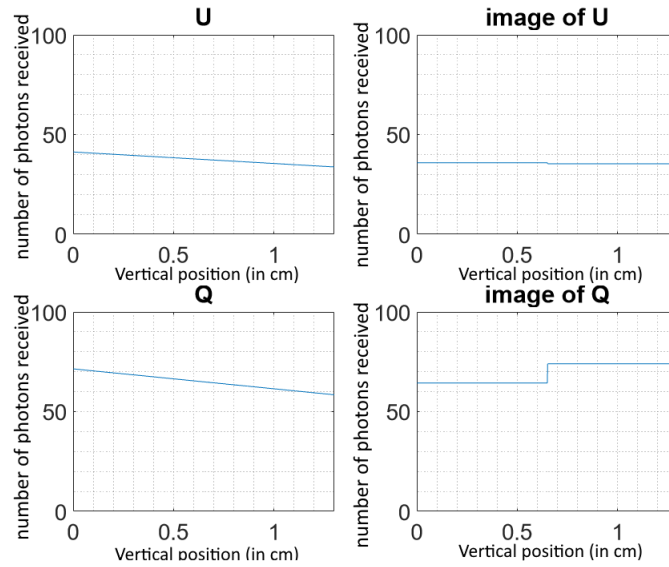


Figure 8.4: U (upper graphs) and Q (lower graphs) values before and after the instrument when we subdivide the detector output signal in two blocks before analysis

The values of the first block are as expected, averaged values of the initial ones, but the outputs of the second block are off. This is due to the fact that the point where we subdivide the signal has an impact on the reconstructed parameters: As seen in section 6.5 with the parallel and perpendicular polarisation, the oscillation is the same but the output signal is shifted. This means that if we want to implement spatial resolution by analysing blocks of the output signal, we have to be very careful with the position of the subdivision, or suffer false results. This could be investigated more deeply in a future study.

9 Conclusion

We can see that the instrument is more adapted for the study of uniform signals (as other signals are averaged), but if we consider that we observe a small part of the sky, a uniform entry signal remains a good approximation.

In the end, this instrument can perceive auroral light polarisation and has a higher theoretical measurement precision than the previous ones, but it may encounter issues at very low light level, as the number of detected photons becomes low and the influence of the noise becomes high.

It may show better results for luminous events than the instruments used previously, since it allows us to record all polarisation states simultaneously. However for faint auroras the performance may not be better, if even reaching the same precision as the other instruments.

Another aspect that has been raised near the end of this work is the constraints linked with the manufacture of such optical elements. If we consider the initial previsions, the dimensions of our instrument are quite small: With its 1.3 cm height, the length of the three wedges would be a bit less than a millimetre.

Manufacturing small angles (1.8 and 3.2 degrees) at such a small scale is not possible yet, if possible at all. We thus have to change the setup to replace the uniform slope of the wedges with a discrete width change (a stair shape). This will cause the retardance to change by discrete steps and the result should show the same output as if we lowered the number of pixels. The main issue that directly rise with this new setup is that by changing the orientation of the contact surface, the risk of straylight increases. More precisely the risk of ghost (unwanted secondary image).

References

- [1] Bogdan Vasilescu. “Development of a spectropolarimeter for space use”. In: (June 2019), p. 150.
- [2] Samy El-Jaby and Richard Richardson. “Monte Carlo simulations of the secondary neutron ambient and effective dose equivalent rates from surface to suborbital altitudes and low Earth orbit”. In: *Life Sciences in Space Research* 6 (May 2015). DOI: 10.1016/j.lssr.2015.05.001.
- [3] National Institute of Standards and Technology. *Atomic Spectra Database*. <https://www.nist.gov/pml/atomic-spectra-database>. Oct. 2020.
- [4] *Trapped particle radiation models*. <https://www.spennis.oma.be/help/background/traprad/traprad.html>. Apr. 2018.
- [5] Štěpán Kunc. “Study of the Magnetically Induced QED Birefringence of the Vacuum in experiment OSQAR”. PhD thesis. Apr. 2018.
- [6] Dennis H Goldstein. “Polarized Light, Third Edition”. In: (), p. 786.
- [7] Jean Lilensten et al. “The thermospheric auroral red line polarization: confirmation of detection and first quantitative analysis”. In: *Journal of Space Weather and Space Climate* 3 (2013), A01. ISSN: 2115-7251. DOI: 10.1051/swsc/2012023. URL: <http://www.swsc-journal.org/10.1051/swsc/2012023> (visited on 02/13/2021).
- [8] Jean Lilensten et al. “The auroral red line polarisation: modelling and measurements”. In: *Journal of Space Weather and Space Climate* 5 (2015), A26. ISSN: 2115-7251. DOI: 10.1051/swsc/2015027. URL: <http://www.swsc-journal.org/10.1051/swsc/2015027> (visited on 02/13/2021).
- [9] Jean Lilensten et al. “The thermospheric auroral red line Angle of Linear Polarization: AURORAL ANGLE OF LINEAR POLARIZATION”. In: *Journal of Geophysical Research: Space Physics* 121.7 (July 2016), pp. 7125–7134. ISSN: 21699380. DOI: 10.1002/2016JA022941. URL: <http://doi.wiley.com/10.1002/2016JA022941> (visited on 02/13/2021).
- [10] Léo Bosse et al. “On the nightglow polarisation for space weather exploration”. In: *Journal of Space Weather and Space Climate* 10 (2020), p. 35. ISSN: 2115-7251. DOI: 10.1051/swsc/2020036. URL: <https://www.swsc-journal.org/10.1051/swsc/2020036> (visited on 05/14/2021).

- [11] Mathieu Barthelemy et al. “Measurement of the polarisation in the auroral N_2^+ 427.8 nm band”. In: *Journal of Space Weather and Space Climate* 9 (2019), A26. ISSN: 2115-7251. DOI: 10.1051/swsc/2019024. URL: <https://www.swsc-journal.org/10.1051/swsc/2019024> (visited on 05/14/2021).
- [12] V. Bommier et al. “The theoretical impact polarization of the O I 6300 Å red line of Earth aurorae”. In: *Annales Geophysicae* 29.1 (Jan. 10, 2011), pp. 71–79. ISSN: 1432-0576. DOI: 10.5194/angeo-29-71-2011. URL: <https://angeo.copernicus.org/articles/29/71/2011/> (visited on 06/07/2021).
- [13] Edward Collett. *Field Guide to Polarization*. SPIE, Sept. 26, 2005. ISBN: 978-0-8194-7820-7. DOI: 10.1117/3.626141. URL: <https://spiedigitallibrary.org/ebooks/FG/Field-Guide-to-Polarization/eISBN-9780819478207/10.1117/3.626141> (visited on 02/13/2021).
- [14] William Sparks et al. “Compact and robust method for full Stokes spectropolarimetry”. In: *Applied Optics* 51.22 (Aug. 1, 2012), p. 5495. ISSN: 1559-128X, 2155-3165. DOI: 10.1364/AO.51.005495. URL: <https://www.osapublishing.org/abstract.cfm?URI=ao-51-22-5495> (visited on 02/13/2021).
- [15] Bogdan Vasilescu, Yaël Nazè, and Jérôme Loicq. “Solution uniqueness and noise impact in a static spectropolarimeter based on birefringent prisms for full Stokes parameter retrieval”. In: *Journal of Astronomical Telescopes, Instruments, and Systems* 6.2 (Apr. 23, 2020), p. 1. ISSN: 2329-4124. DOI: 10.1117/1.JATIS.6.2.028001. URL: <https://www.spiedigitallibrary.org/journals/Journal-of-Astronomical-Telescopes-Instruments-and-Systems/volume-6/issue-02/028001/Solution-uniqueness-and-noise-impact-in-a-static-spectropolarimeter-based/10.1117/1.JATIS.6.2.028001.full> (visited on 02/13/2021).
- [16] Thomas Oksenhendler. “Self-referenced spectral interferometry theory”. In: (Apr. 2012).
- [17] H. M. Schmid et al. “SPHERE / ZIMPOL high resolution polarimetric imager. I. System overview, PSF parameters, coronagraphy, and polarimetry”. In: *Astronomy & Astrophysics* 619 (Nov. 2018), A9. ISSN: 0004-6361, 1432-0746. DOI: 10.1051/0004-6361/201833620. arXiv: 1808.05008. URL: <http://arxiv.org/abs/1808.05008> (visited on 07/21/2021).
- [18] S. K. Solanki et al. “The Polarimetric and Helioseismic Imager on Solar Orbiter”. In: *Astronomy & Astrophysics* 642 (Oct. 2020), A11. ISSN: 0004-6361, 1432-0746. DOI: 10.1051/0004-6361/201935325. URL: <https://www.aanda.org/10.1051/0004-6361/201935325> (visited on 07/22/2021).

- [19] Aaldert van Amerongen et al. “SPEXone: A compact multi-angle spectropolarimeter”. In: (), p. 13.
- [20] Jeremy Werdell. *PACE Plankton, Aerosol, Cloud, ocean Ecosystem*. <https://pace.oceansciences.org/spexone.htm>. July 2021.
- [21] “INTRODUCTION TO SPECTROPOLARIMETRY”. In: (), p. 245.
- [22] Martin Pertenais. “Spectropolarimétrie stellaire UV et visible depuis l’espace”. PhD thesis, p. 131.
- [23] Martin Pertenais et al. “Static spectropolarimeter concept adapted to space conditions and wide spectrum constraints”. In: *Applied Optics* 54.24 (Aug. 20, 2015), p. 7377. ISSN: 0003-6935, 1539-4522. DOI: 10.1364/AO.54.007377. arXiv: 1507.06894. URL: <http://arxiv.org/abs/1507.06894> (visited on 02/13/2021).
- [24] Felix Jottrand. “Study, development and tests of two methods to determine the degree of linear polarization of auroral light”. In: (June 2020), p. 93.
- [25] R. H. Eather. “Auroral proton precipitation and hydrogen emissions”. In: *Reviews of Geophysics* 5.3 (1967), p. 207. ISSN: 8755-1209. DOI: 10.1029/RG005i003p00207. URL: <http://doi.wiley.com/10.1029/RG005i003p00207> (visited on 05/25/2021).
- [26] C. W. Gartlein and G. Sprague. “Hydrogen in auroras”. In: *Journal of Geophysical Research* 62.4 (Dec. 1957), pp. 521–526. ISSN: 01480227. DOI: 10.1029/JZ062i004p00521. URL: <http://doi.wiley.com/10.1029/JZ062i004p00521> (visited on 05/25/2021).
- [27] William B. Sparks, Thomas A. Germer, and Rebecca M. Sparks. “Classical Polarimetry with a Twist: A Compact, Geometric Approach”. In: *Publications of the Astronomical Society of the Pacific* 131.1001 (July 1, 2019), p. 075002. ISSN: 0004-6280, 1538-3873. DOI: 10.1088/1538-3873/ab1933. URL: <https://iopscience.iop.org/article/10.1088/1538-3873/ab1933> (visited on 07/21/2021).
- [28] Nathan Hagen and Eustace L Dereniak. “Snapshot-Imaging Spectropolarimeter”. In: (), p. 21.
- [29] Wei Ting Chen et al. “Integrated Plasmonic Metasurfaces for Spectropolarimetry”. In: *Nanotechnology* 27.22 (June 3, 2016), p. 224002. ISSN: 0957-4484, 1361-6528. DOI: 10.1088/0957-4484/27/22/224002. arXiv: 1510.04110. URL: <http://arxiv.org/abs/1510.04110> (visited on 07/21/2021).

- [30] Meredith K. Kupinski et al. “Angle of linear polarization images of outdoor scenes”. In: *Optical Engineering* 58.8 (June 11, 2019), p. 1. ISSN: 0091-3286. DOI: 10.1117/1.0E.58.8.082419. URL: <https://www.spiedigitallibrary.org/journals/optical-engineering/volume-58/issue-08/082419/Angle-of-linear-polarization-images-of-outdoor-scenes/10.1117/1.0E.58.8.082419.full> (visited on 07/21/2021).
- [31] K. Albert et al. “Performance analysis of the SO/PHI software framework for on-board data reduction”. In: *arXiv:1905.08690 [astro-ph]* (May 21, 2019). arXiv: 1905.08690. URL: <http://arxiv.org/abs/1905.08690> (visited on 07/22/2021).
- [32] Christian Thalmann et al. “SPHERE ZIMPOL: overview and performance simulation”. In: SPIE Astronomical Telescopes + Instrumentation. Ed. by Ian S. McLean and Mark M. Casali. Marseille, France, July 12, 2008, 70143F. DOI: 10.1117/12.789158. URL: <http://proceedings.spiedigitallibrary.org/proceeding.aspx?doi=10.1117/12.789158> (visited on 07/22/2021).
- [33] Bogdan Vasilescu et al. “Development of a space spectropolarimeter for full stokes parameters retrieval”. In: *International Conference on Space Optics — ICSO 2020*. International Conference on Space Optics — ICSO 2021. Ed. by Zoran Sodnik, Bruno Cugny, and Nikos Karafolas. Online Only, France: SPIE, June 11, 2021, p. 89. ISBN: 978-1-5106-4548-6 978-1-5106-4549-3. DOI: 10.1117/12.2599427. URL: <https://www.spiedigitallibrary.org/conference-proceedings-of-spie/11852/2599427/Development-of-a-space-spectropolarimeter-for-full-stokes-parameters-retrieval/10.1117/12.2599427.full> (visited on 07/22/2021).
- [34] Francisco A. Iglesias and Alex Feller. “Instrumentation for solar spectropolarimetry: state of the art and prospects”. In: *Optical Engineering* 58.8 (Apr. 27, 2019), p. 1. ISSN: 0091-3286. DOI: 10.1117/1.0E.58.8.082417. URL: <https://www.spiedigitallibrary.org/journals/optical-engineering/volume-58/issue-08/082417/Instrumentation-for-solar-spectropolarimetry--state-of-the-art-and/10.1117/1.0E.58.8.082417.full> (visited on 07/22/2021).
- [35] Tianlei Ning et al. “Single-shot measurement of polarization state at low light field using Mueller-mapping star test polarimetry”. In: *Optics Communications* 496 (Oct. 2021), p. 127130. ISSN: 00304018. DOI: 10.1016/j.optcom.2021.127130. URL: <https://linkinghub.elsevier.com/retrieve/pii/S0030401821003795> (visited on 07/22/2021).

- [36] Frans Snik, Theodora Karalidi, and Christoph U. Keller. “Spectral modulation for full linear polarimetry”. In: *Applied Optics* 48.7 (Mar. 1, 2009), p. 1337. ISSN: 0003-6935, 1539-4522. DOI: 10.1364/AO.48.001337. arXiv: 0903.2735. URL: <http://arxiv.org/abs/0903.2735> (visited on 07/23/2021).